Microfluidics and Nanofluidics (2018) 22:112
https://doi.org/10.1007/s10404-018-2133-6

RESEARCH PAPER

Electrokinetics in nanochannels grafted with poly-zwitterionic brushes

Guang Chen[1] · Jahin Patwary[1] · Harnoor Singh Sachar[1] · Siddhartha Das[1]

Received: 7 June 2018 / Accepted: 21 September 2018 / Published online: 5 October 2018

Abstract
In this paper, we compute the electrokinetic transport in soft nanochannels grafted with poly-zwitterionic (PZI) brushes. The transport is induced by an external pressure gradient, which drives the ionic cloud (in the form of an electric double layer or EDL) at the brush surfaces to induce an electric field that drives an induced electroosmotic transport. We characterize the overall transport by quantifying this electric field, overall flow velocity, and the energy conversion associated with the development of the electric field and a streaming current. We specially focus on how the ability of the PZI to ionize and demonstrate a significant charge at both large and small pH can be efficiently maneuvered to develop a liquid transport, an electric field, and an electrokinetically induced power across a wide range of pH values.

1 Introduction

Functionalizing nanoscale interfaces (e.g., walls of nanochannels or the surfaces of nanoparticles) with polymer and polyelectrolyte (PE) brushes (Alexander 1977; Gennes 1976, 1980; Netz and Andelman 2003; Das et al. 2015; Milner 1991) has been extensively used for a myriad of applications such as targeted drug delivery (Knop et al. 2010; Suk et al. 2015), oil recovery (ShamsiJazeyi et al. 2014), ion and biosensing (Groot et al. 2013; Yameen et al. 2009; Ali et al. 2008, 2010a; Umehara et al. 2009), current rectification (Ali et al. 2010b), fabrication of nanofluidic diodes (Vilozny et al. 2013; Ali et al. 2009) and nanoactuators (Moya et al. 2005), and many more. The central idea that drives most of these applications is how the brushes respond to the environmental stimuli (e.g., local pH, salt concentration, temperature, etc.) and regulate the transport of different species. Under these conditions, there have been significant efforts in studying the ion and liquid transport in nanochannels or nanopores grafted with PE brushes that are pH-responsive (Groot et al. 2013; Yameen et al. 2009; Chen and Das 2015a, b, 2017a; Patwary et al. 2015; Li et al. 2016; Milne et al. 2014; Yameen et al. 2009; Tagliazucchi et al. 2010; Lin et al. 2016; Ma et al. 2015; Xue et al. 2014; Zhou et al. 2016; Ali et al. 2008; Gilles et al. 2016; Tagliazucchi and Szleifer 2012).

Poly-zwitterion (PZI) is a particular type of PE that contains both negative and positive sites (Lowe and McCormick 2006). These sites typically ionize as a function of the local pH; however, the extent of ionization of the positive site and that of the negative site are different at different pH. Therefore, at a given pH, the PZI is either negatively or positively charged. The PZI molecules have been extensively employed in a large number of applications, such as the fabrication of "smart" materials with environmental–stimuli-responsive switchable properties (Ilcikova et al. 2015), sub-surface imaging and oil recovery (Urena-Benavides et al. 2016), capturing chemical moieties (Saleh et al. 2017), drug delivery (Xiao et al. 2012), biomacromolecular separation (Zhao et al. 2017), removal of organic pollutants (Monteil et al. 2016), use as heterogeneous catalysts (Fidale et al. 2013), and many more. In this paper, we study the electrohydrodynamics in a nanochannel grafted with such PZI molecules existing in a "brush" like state. There have been significant previous efforts where interfaces grafted with such PZI brushes have been used for a variety of applications such as triggering extreme lubrication (Chen et al. 2009, 2011), reversible switching of the surface wettability (Azzaroni et al. 2006; Cheng et al. 2008), inducing repeatable adhesion (Kobayashi and Takahara 2013), fabrication of antifouling surfaces (Higaki et al. 2016), regulating ion selectivity in nanopores (Zeng et al. 2015), etc. However, this is for the first time that its effect in electrohydrodynamics and

✉ Siddhartha Das
sidd@umd.edu

[1] Department of Mechanical Engineering, University of Maryland, College Park, MD 20742, USA

electrokinetic energy conversion in a brush-grafted nanochannel is being probed.

Our paper provides detailed calculations of the pH-responsive electric double layer electrostatics and how that electrostatics regulates the flow and the overall electrokinetics in the presence of an externally imposed pressure-driven transport. We calculate the electric field induced by this pressure-driven transport and how this electric field and the induced streaming current couple to generate an electrokinetic power. This power generation is an example of electrochemomechanical energy conversion and has been touted as one of the key applications of nanochannel electrokinetic transport (Patwary et al. 2015; Chanda et al. 2014; Chen and Das 2015d; Chen et al. 2018; Daiguji et al. 2004; Nguyen et al. 2013; Heyden et al. 2006a, 2007). Here, we establish that working with the PZI brush allows for the generation of the large electrokinetic power across a wide range of pH (i.e., for both large and small pH). In other words, this paper points to a new design information in the context of electrokinetic power generation in soft or PE brush-grafted nanochannels—a single design allows the flexibility of generating electrokinetic power across a wide spectrum of pH, which is not possible for brush-free nanochannels (Daiguji et al. 2004; Nguyen et al. 2013; Heyden et al. 2006a, 2007) or nanochannels grafted with the PE (and not PZI) brushes (Patwary et al. 2015).

2 Theory

2.1 Electrostatics

We consider a pressure-driven transport in a nanochannel of height $2h$ and grafted with a layer of PZI brushes of constant height d (with $d < h$) (see Fig. 1). To obtain the overall transport, we would have to first get the electrostatics of the EDL induced by the brushes. Considering the bottom half of a nanochannel (i.e., $-h \le y \le 0$), the free-energy functional dictating the EDL electrostatics can be expressed as follows:

$$\mathcal{F} = \int f\left[\psi, n_{\pm}, n_{\mathrm{H}^+}, n_{\mathrm{OH}^-}\right] \mathrm{d}^3\mathbf{r}, \tag{1}$$

where $\mathrm{d}^3\mathbf{r}$ represents the volumetric integration, ψ is the electrostatic potential, n_i is the number density of the ion i ($i = \pm, \mathrm{H}^+, \mathrm{OH}^-$), and f is the free-energy density expressed as follows:

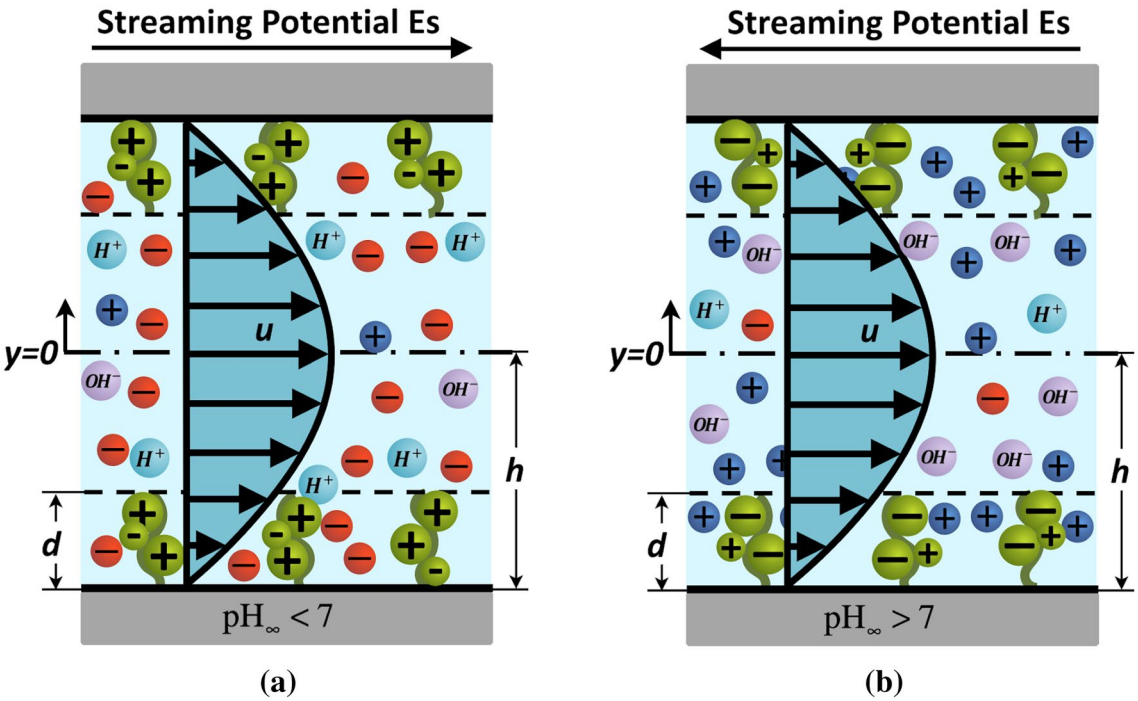

Fig. 1 Schematic showing the pressure-driven transport and induced electric field in a PZI brush-grafted nanochannels. The PZI brush is positively charged for small pH ($\mathrm{pH}_\infty < 7$) (**a**) and negatively charged for large pH ($\mathrm{pH}_\infty > 7$) (**b**), leading to the generation of a positive streaming potential (**a**) and a negative streaming potential (**b**). In this figure, the ionic charges of the PZI are represented in green (for $\mathrm{pH}_\infty < 7$, the PZI is more positive, while, for $\mathrm{pH}_\infty > 7$, the PZI is more negative), the cations (from the salt) in blue (dark), the anions (from the salt) in orange, the H^+ ions in blue (light), and the OH ions in purple. (Color figure online)

$$
\begin{aligned}
f &= k_B T\left[n_+\left(\ln\left(\frac{n_+}{n_{+,\infty}}\right)-1\right)+n_-\left(\ln\left(\frac{n_-}{n_{-,\infty}}\right)-1\right)+n_{H^+}\left(\ln\left(\frac{n_{H^+}}{n_{H^+,\infty}}\right)-1\right)+n_{OH^-}\left(\ln\left(\frac{n_{OH^-}}{n_{OH^-,\infty}}\right)-1\right)\right]\\
&\quad-\frac{\epsilon_0\epsilon_r}{2}|\nabla\psi|^2+e\psi\left(n_+-n_-+n_{H^+}-n_{OH^-}-\varphi n_{A^-}+\varphi n_{BH^+}\right)\quad[\text{for}\quad -h\le y\le -h+d],\\
f &= k_B T\left[n_+\left(\ln\left(\frac{n_+}{n_{+,\infty}}\right)-1\right)+n_-\left(\ln\left(\frac{n_-}{n_{-,\infty}}\right)-1\right)+n_{H^+}\left(\ln\left(\frac{n_{H^+}}{n_{H^+,\infty}}\right)-1\right)+n_{OH^-}\left(\ln\left(\frac{n_{OH^-}}{n_{OH^-,\infty}}\right)-1\right)\right]\\
&\quad-\frac{\epsilon_0\epsilon_r}{2}|\nabla\psi|^2+e\psi\left(n_+-n_-+n_{H^+}-n_{OH^-}\right)\quad[\text{for}\quad -h+d\le y\le 0].
\end{aligned}
\tag{2}
$$

In Eq. (2), $k_B T$ is the thermal energy, e is the electronic charge, ϵ_0 is the permittivity of free space, ϵ_r is the relative permittivity of the medium, e is the electronic charge, $n_{i,\infty}$ is the bulk number density of the ions i ($i = \pm, H^+, OH^-$), and φ is the dimensionless distribution of the PZI chargeable sites (PZICS) of a given brush molecule. Here, we consider identical relative permittivities both inside and outside the brush layer very much similar to the previous studies (see review article in Das et al. 2015). Of course, one can consider an even more rigorous model by accounting for the fact that the relative permittivity inside the brush is different from that outside the brush necessitating the consideration of the ion-partitioning effect (Poddar et al. 2016). Typically, such a consideration will become important for a very dense system of brushes. We do not consider such a dense system, where the penetration depth will be very small enforcing virtually no flow inside the brush layer. With the brush being a PZI brush, the PZICS will simultaneously consist of a negative charge centre and a positive charge centre. The formation of the negative charge centre can be attributed to the ionization of an acidic functional group HA ($HA \leftrightarrow H^+ + A^-$; ionization constant K_a having the units of moles/liter) yielding A^- ions. On the other hand, the formation of the positive charge centre can be attributed to the ionization of a basic functional group B ($B + H_2O \leftrightarrow BH^+ + OH^-$; ionization constant K_b having the units of moles/liter) yielding BH^+ ions. Under these conditions, the number densities (in units of $1/m^3$) of the ionic groups of the PZI molecule (namely n_{A^-} and n_{BH^+}) can be expressed as follows [very similar to the form proposed previously (Zeng et al. 2015)]:

$$
n_{A^-} = \frac{K'_a \gamma_a}{K'_a + n_{H^+}},
\tag{3}
$$

$$
n_{BH^+} = \frac{K'_b \gamma_b}{K'_b + n_{OH^-}},
\tag{4}
$$

where γ_a and γ_b are the maximum site densities of acidic and basic functional groups of the PZI, $K'_a = 10^3 N_A K_a$, and $K'_b = 10^3 N_A K_b$ (N_A is the Avogadro number). Of course, Eqs. (2)–(4) show the dependence of the overall problem on the pH of the system.

The equilibrium electrostatic potential and the concentration distribution of different ions can be obtained by minimizing $\mathcal{F}$. Minimizing $\mathcal{F}$ with respect to ψ, we get (considering only the bottom half of the nanochannel):

$$
\begin{aligned}
\frac{\delta\mathcal{F}}{\delta\psi}=0\Rightarrow\frac{\partial f}{\partial\psi}-\frac{\mathrm{d}}{\mathrm{d}y}\left(\frac{\partial f}{\partial\psi'}\right)\Rightarrow\frac{\mathrm{d}^2\psi}{\mathrm{d}y^2}&=\frac{e\left(n_- - n_+ + n_{OH^-} - n_{H^+} + \varphi n_{A^-} - \varphi n_{BH^+}\right)}{\epsilon_0\epsilon_r}\quad[\text{for}\quad -h\le y\le -h+d],\\
\frac{\delta\mathcal{F}}{\delta\psi}=0\Rightarrow\frac{\partial f}{\partial\psi}-\frac{\mathrm{d}}{\mathrm{d}y}\left(\frac{\partial f}{\partial\psi'}\right)\Rightarrow\frac{\mathrm{d}^2\psi}{\mathrm{d}y^2}&=\frac{e\left(n_- - n_+ + n_{OH^-} - n_{H^+}\right)}{\epsilon_0\epsilon_r}\quad[\text{for}\quad -h+d\le y\le 0].
\end{aligned}
\tag{5}
$$

Minimizing $\mathcal{F}$, with respect to $n_\pm$, n_{H^+} and n_{OH^-}, we get the expression of the ion distributions:

$$
\frac{\delta F}{\delta n_\pm}=0\Rightarrow n_\pm=\left(n_{\pm,\infty}\right)\exp\left(\mp\frac{e\psi}{k_B T}\right)\quad[\text{for}\ \ y\ge -h],
\tag{6}
$$

$$
\begin{aligned}
\frac{\delta F}{\delta n_{OH^-}}=0\Rightarrow n_{OH^-}&=\left(n_{OH^-,\infty}\right)\exp\left[\frac{e\psi}{k_B T}\left(1+\varphi\frac{K'_b\gamma_b}{\left(K'_b+n_{OH^-}\right)^2}\right)\right]\quad[\text{for}\quad -h\le y\le -h+d],\\
\frac{\delta F}{\delta n_{OH^-}}=0\Rightarrow n_{OH^-}&=\left(n_{OH^-,\infty}\right)\exp\left(\frac{e\psi}{k_B T}\right)\quad[\text{for}\quad -h+d\le y\le 0].
\end{aligned}
\tag{7}
$$

and

$$\frac{\delta F}{\delta n_{\mathrm{H}^+}} = 0 \Rightarrow n_{\mathrm{H}^+} = \left(n_{\mathrm{H}^+,\infty}\right) \exp\left[-\frac{e\psi}{k_{\mathrm{B}}T}\left(1 + \varphi\frac{K'_{\mathrm{a}}\gamma_{\mathrm{a}}}{\left(K'_{\mathrm{a}} + n_{\mathrm{H}^+}\right)^2}\right)\right] \quad [\text{for} \quad -h \le y \le -h+d],$$
$$\frac{\delta F}{\delta n_{\mathrm{H}^+}} = 0 \Rightarrow n_{\mathrm{H}^+} = \left(n_{\mathrm{H}^+,\infty}\right) \exp\left(-\frac{e\psi}{k_{\mathrm{B}}T}\right) \quad [\text{for} \quad -h+d \le y \le 0]. \tag{8}$$

Here, $n_{\pm,\infty}$ are the bulk number density of the electrolyte ions, $n_{\mathrm{H}^+,\infty} = 10^3 N_{\mathrm{A}} 10^{-\mathrm{pH}_\infty}$ is the bulk number density of hydrogen ions (pH_∞ is the bulk pH), and $n_{\mathrm{OH}^-,\infty} = 10^3 N_{\mathrm{A}} 10^{-\mathrm{pOH}_\infty}$ (pOH_∞ is the bulk pOH) is the bulk number density of the hydroxide ions and $\mathrm{pH}_\infty + \mathrm{pOH}_\infty = 14$. The bulk number densities are the number densities of the ions in the microchannel reservoirs (where $\psi = 0$) connecting the nanochannel (Baldessari and Santiago 2008; Das et al. 2013, 2014). Solution of ψ can be obtained by first using Eqs. (6)–(8) to replace the ion number densities appearing in Eq. (5), and then solving the resultant differential equation in ψ in the presence of the boundary conditions expressed in the following:

$$\left(\frac{\mathrm{d}\psi}{\mathrm{d}y}\right)_{y=0} = 0, \quad (\psi)_{y=(-h+d)^+} = (\psi)_{y=(-h+d)^-}, \quad \left(\frac{\mathrm{d}\psi}{\mathrm{d}y}\right)_{y=(-h+d)^+} = \left(\frac{\mathrm{d}\psi}{\mathrm{d}y}\right)_{y=(-h+d)^-}, \quad \left(\frac{\mathrm{d}\psi}{\mathrm{d}y}\right)_{y=-h} = 0. \tag{9}$$

The boundary conditions in Eq. (9), respectively, represent the condition of an uncharged nanochannel wall (first equation of Eq. 9), identical potential and potential gradient at the brush–liquid interface at $y = -h + d$ (second and third equations of Eq. 9), and symmetry at the nanochannel centreline (final equation of Eq. 9). The critical thing to note here is that this differential equation in ψ will also contain the unresolved expression for n_{H^+} and n_{OH^-}; this stems from the fact that, while the expressions for the number densities of $n_{\pm}$ are explicit in ψ (see Eqs. 6, 7), n_{H^+} and n_{OH^-} are implicit in ψ (see Eqs. 7, 8). Therefore, we shall have a set of equations for ψ, n_{H^+}, and n_{OH^-} that will be needed to be solved simultaneously. Finally, we would like to point out that this coupled solution of ψ and n_{H^+} as well as ψ and n_{OH^-} will require the information on the distribution of $\varphi = \varphi(y)$. We shall discuss this choice of $\varphi(y)$ later. As already mentioned, the first equation of Eq. (9) describes the grafting wall as an uncharged wall. We intentionally considered such an uncharged wall and not a more typical silica wall. A silica wall would typically show a negative charge density for an acidic pH (Behrens and Grier 2001). On the other hand, for such an acidic pH, the

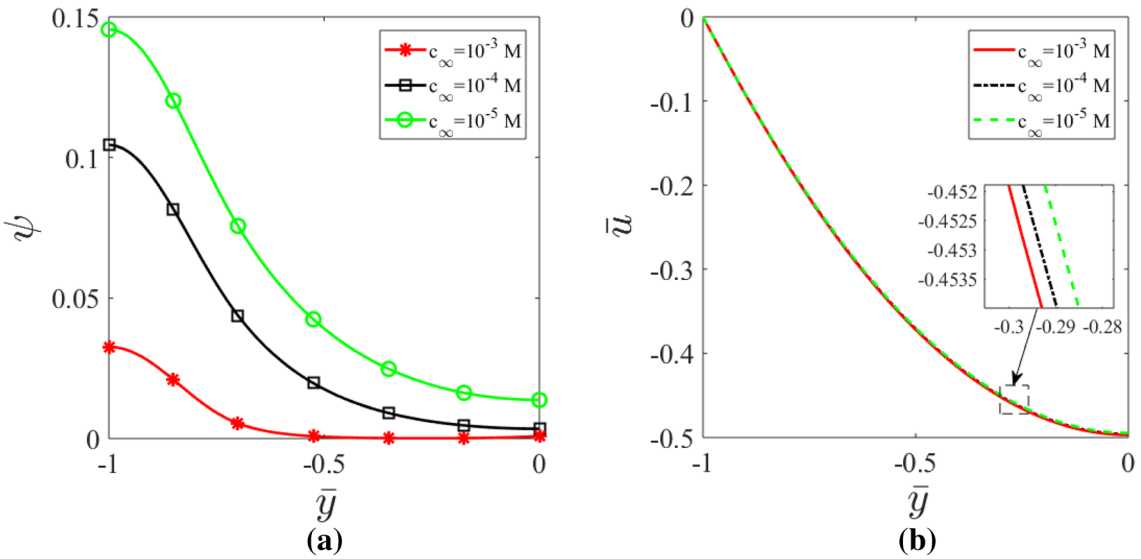

Fig. 2 Transverse variation of **a** dimensionless electrostatic potential $\bar{\psi}$ and **b** dimensionless velocity profile $\bar{u}$ for different values of bulk salt concentration c_∞. Other parameters for this figure are $\mathrm{pH}_\infty = 4$ (or bulk pH), $\mathrm{p}K_{\mathrm{a}} = 4$, $\mathrm{p}K_{\mathrm{b}} = 4$, $\bar{d} = 0.3$, $\gamma_{\mathrm{a}} = 10^{-4}$ M, $\gamma_{\mathrm{b}} = 10^{-4}$ M, $\bar{\alpha} = 1$, $u_{\mathrm{r}} = 1$, $R_i = 1$, $\frac{N_p a^3 \sigma}{d} = 1$, $h = 100$ nm, $k_{\mathrm{B}} = 1.38 \times 10^{-23}$ J/K, $T = 300$ K, $e = 1.6 \times 10^{-19}$ C, $\epsilon_0 = 8.854 \times 10^{-12}$ F/m, a = 1 nm, and $\epsilon_{\mathrm{r}} = 79.8$

brushes are positively charged (see Fig. 2, later). Under such conditions, the brushes will get attracted to the wall forming a "mushroom"-like or "pancake"-like configuration (Das et al. 2015), i.e., deviate from the brush-like configuration making our analysis invalid.

PZI brush layer in an acidic solution

We first consider the PZI brush layer dissociation in an acidic solution. We consider that the acid furnishes the same anion as the salt. As a consequence, the bulk number density of the salt anion will be $n_\infty + n_{H^+,\infty}$. Under this condition, we can non-dimensionalize equations (7, 8) as well as the equation that results from using Eqs. (6)–(8) to replace the ion number densities in Eq. (5) to yield:

$$\left(\frac{d\bar{\psi}}{d\bar{y}}\right)_{\bar{y}=0} = 0, \quad (\bar{\psi})_{\bar{y}=(-1+\bar{d})^+} = (\bar{\psi})_{\bar{y}=(-1+\bar{d})^-},$$
$$\left(\frac{d\bar{\psi}}{d\bar{y}}\right)_{\bar{y}=(-1+\bar{d})^+} = \left(\frac{d\bar{\psi}}{d\bar{y}}\right)_{\bar{y}=(-1+\bar{d})^-}, \quad \left(\frac{d\bar{\psi}}{d\bar{y}}\right)_{\bar{y}=-1} = 0. \tag{13}$$

In the above equations, $\bar{y} = y/h$, $\bar{\lambda} = \lambda/h$ ($\lambda = \sqrt{\frac{\epsilon_0 \epsilon_r k_B T}{2e^2 \sum_i n_{i,\infty}}}$ is the EDL thickness), $\bar{d} = d/h$, $\bar{\psi} = e\psi/(k_B T)$, $\bar{n}_{H^+} = n_{H^+}/n_\infty$, $\bar{n}_{OH^-} = n_{OH^-}/n_\infty$, $\bar{n}_{H^+,\infty} = n_{H^+,\infty}/n_\infty$, $\bar{n}_{OH^-,\infty} = n_{OH^-,\infty}/n_\infty$, $\bar{K}'_a = K'_a/n_\infty$, and $\bar{\gamma}_a = \gamma_a/n_\infty$. Here, $n_\infty = 10^3 N_A c_\infty$ (c_∞ is the concentration in M, while n_∞ is the number density in $1/m^3$). In addition, as established in our previous studies (Chen and Das 2015b, c), we can consider a cubic profile for $\varphi(y)$, that is

$$\frac{d^2\bar{\psi}}{d\bar{y}^2} = \frac{1}{2\bar{\lambda}^2}\left[\bar{n}_- - \bar{n}_+ + \bar{n}_{OH^-} - \bar{n}_{H^+} + \varphi\bar{n}_{A^-} - \varphi\bar{n}_{BH^+}\right] \quad [\text{for } -1 \le \bar{y} \le -1+\bar{d}]$$
$$= \frac{1}{2\bar{\lambda}^2}\left[\left(1+\bar{n}_{H^+,\infty}\right)\exp(\bar{\psi}) - \exp(-\bar{\psi}) + \bar{n}_{OH^-} - \bar{n}_{H^+} + \varphi\frac{\bar{K}'_a\bar{\gamma}_a}{\bar{K}'_a + \bar{n}_{H^+}} - \varphi\frac{\bar{K}'_b\bar{\gamma}_b}{\bar{K}'_b + \bar{n}_{OH^-}}\right], \tag{10}$$
$$\frac{d^2\bar{\psi}}{d\bar{y}^2} = \frac{1}{2\bar{\lambda}^2}\left[\bar{n}_- - \bar{n}_+ + \bar{n}_{OH^-} - \bar{n}_{H^+}\right] \quad [\text{for } -1+\bar{d} \le \bar{y} \le 0]$$
$$= \frac{1}{2\bar{\lambda}^2}\left[\left(1+\bar{n}_{H^+,\infty}\right)\exp(\bar{\psi}) - \exp(-\bar{\psi}) + \left(\bar{n}_{OH^-,\infty}\right)\exp(\bar{\psi}) - \left(\bar{n}_{H^+,\infty}\right)\exp(-\bar{\psi})\right].$$

$$\bar{\psi} = -\frac{\ln\left(\frac{\bar{n}_{H^+}}{\bar{n}_{H^+,\infty}}\right)}{1 + \frac{\bar{K}'_a\bar{\gamma}_a\varphi(\bar{y})}{\left(\bar{K}'_a+\bar{n}_{H^+}\right)^2}} \quad [\text{for } -1 \le \bar{y} \le -1+\bar{d}],$$
$$\bar{\psi} = -\ln\left(\frac{\bar{n}_{H^+}}{\bar{n}_{H^+,\infty}}\right) \quad [\text{for } -1+\bar{d} \le \bar{y} \le 0]. \tag{11}$$

$$\bar{\psi} = \frac{\ln\left(\frac{\bar{n}_{OH^-}}{\bar{n}_{OH^-,\infty}}\right)}{1 + \frac{\bar{K}'_b\bar{\gamma}_b\varphi(\bar{y})}{\left(\bar{K}'_b+\bar{n}_{OH^-}\right)^2}} \quad [\text{for } -1 \le \bar{y} \le -1+\bar{d}],$$
$$\bar{\psi} = \ln\left(\frac{\bar{n}_{OH^-}}{\bar{n}_{OH^-,\infty}}\right) \quad [\text{for } -1+\bar{d} \le \bar{y} \le 0]. \tag{12}$$

The corresponding dimensionless boundary conditions obtained by non-dimensionalizing equation (9) become:

$$\varphi(\bar{y}) = \beta\left(\bar{y}+1-\bar{d}\right)^2\left(\bar{y}+1+\frac{\bar{d}}{2}\right), \tag{14}$$

where $\beta = 4/\bar{d}^3$. We provide a detailed discussion later on this choice of the cubic profile later in Sect. 4.

Furthermore, as we are considering the PZI brush layer dissociation in an acidic solution, the concentration of the OH^- ions would be very small, so that we have $\bar{K}'_b \gg \bar{n}_{OH^-}$, and consequently, Eq. (12) reduces to:

$$\bar{n}_{OH^-} = \left(\bar{n}_{OH^-,\infty}\right)\exp\left[\bar{\psi}\left(1+\varphi\frac{\bar{\gamma}_b}{\bar{K}'_b}\right)\right] \quad [\text{for } -1 \le \bar{y} \le -1+\bar{d}],$$
$$\bar{n}_{OH^-} = \left(\bar{n}_{OH^-,\infty}\right)\exp(\bar{\psi}) \quad [\text{for } -1+\bar{d} \le y \le 0]. \tag{15}$$

Therefore, Eq. (10) can be simplified as follows:

$$\frac{d^2\bar{\psi}}{d\bar{y}^2} = \frac{1}{2\bar{\lambda}^2}\left[\left(1+\bar{n}_{H^+,\infty}\right)\exp(\bar{\psi}) - \exp(-\bar{\psi}) + \left(\bar{n}_{OH^-,\infty}\right)\exp\left[\bar{\psi}\left(1+\varphi\frac{\bar{\gamma}_b}{\bar{K}'_b}\right)\right] - \bar{n}_{H^+} + \varphi\frac{\bar{K}'_a\bar{\gamma}_a}{\bar{K}'_a+\bar{n}_{H^+}} - \varphi\bar{\gamma}_b\right]$$
$$[\text{for } -1 \le \bar{y} \le -1+\bar{d}],$$
$$\frac{d^2\bar{\psi}}{d\bar{y}^2} = \frac{1}{2\bar{\lambda}^2}\left[\left(1+\bar{n}_{H^+,\infty}\right)\exp(\bar{\psi}) - \exp(-\bar{\psi}) + \left(\bar{n}_{OH^-,\infty}\right)\exp(\bar{\psi}) - \left(\bar{n}_{H^+,\infty}\right)\exp(-\bar{\psi})\right] \text{ [for } -1+\bar{d} \le \bar{y} \le 0]. \tag{16}$$

The explicit equilibrium electrostatic potential, H^+, and OH^- ion concentration distributions can be obtained by numerically solving the coupled equations (Eqs. 11, 15, 16) in the presence of the boundary condition expressed in (13).

Poly-zwitterionic brush layer in basic solution

We next consider the case where the PZI brush layer is dissociating in a basic solution. We consider that the base furnishes the same cation as the salt. As a consequence, the bulk number density of the salt cation will be $n_\infty + n_{OH^-,\infty}$.

Furthermore, the solution being basic, we would have $\bar{K}'_a \gg \bar{n}_{H^+}$, and consequently, Eq. (11) reduces to:

$$\bar{n}_{H^+} = \left(\bar{n}_{H^+,\infty}\right)\exp\left[-\bar{\psi}\left(1+\varphi\frac{\bar{\gamma}_a}{\bar{K}'_a}\right)\right] \quad [\text{for } -1 \le \bar{y} \le -1+\bar{d}],$$
$$\bar{n}_{H^+} = \left(\bar{n}_{H^+,\infty}\right)\exp\left(-\bar{\psi}\right) \quad [\text{for } -1+\bar{d} \le y \le 0]. \tag{17}$$

Under these conditions, Eq. (10) can be simplified as follows:

$$\frac{d^2\bar{\psi}}{d\bar{y}^2} = \frac{1}{2\bar{\lambda}^2}\left[\exp\left(\bar{\psi}\right) - \left(1+\bar{n}_{OH^-,\infty}\right)\exp\left(-\bar{\psi}\right) + \bar{n}_{OH^-} - \left(\bar{n}_{H^+,\infty}\right)\exp\left[-\bar{\psi}\left(1+\varphi\frac{\bar{\gamma}_a}{\bar{K}'_a}\right)\right] + \varphi\bar{\gamma}_a - \varphi\frac{\bar{K}'_b\bar{\gamma}_b}{\bar{K}'_b+\bar{n}_{OH^-}}\right]$$
$$[\text{for } -1 \le \bar{y} \le -1+\bar{d}],$$
$$\frac{d^2\bar{\psi}}{d\bar{y}^2} = \frac{1}{2\bar{\lambda}^2}\left[\exp\left(\bar{\psi}\right) - \left(1+\bar{n}_{OH^-,\infty}\right)\exp\left(-\bar{\psi}\right) + \left(\bar{n}_{OH^-,\infty}\right)\exp\left(\bar{\psi}\right) - \left(\bar{n}_{H^+,\infty}\right)\exp\left(-\bar{\psi}\right)\right] [\text{for } -1+\bar{d} \le \bar{y} \le 0]. \tag{18}$$

The explicit equilibrium electrostatic potential, H^+, and OH^- ion concentration distributions can be obtained by numerically solving the coupled equations (Eqs. 12, 17, 18) in the presence of the boundary condition expressed in (13).

2.2 Velocity field

The pressure-driven transport considered here would give rise to an electric field. This electric field will d rive an electroosmotic (EOS) flow, whose direction would always be opposite to the direction of the pressure-driven transport. Considering this overall velocity field (which is a combination of the pressure-driven transport and an EOS flow) to be steady, uni-directional, and hydrodynamically fully developed, we can express it for the channel bottom half as follows:

$$\eta\frac{d^2u}{dy^2} - \frac{dp}{dx} + eE_S(n_+ - n_- + n_{H^+} - n_{OH^-}) - \frac{\eta}{\kappa}u = 0 \quad [-h \le y \le -h+d],$$
$$\eta\frac{d^2u}{dy^2} - \frac{dp}{dx} + eE_S(n_+ - n_- + n_{H^+} - n_{OH^-}) = 0 \quad [-h+d \le y \le 0]. \tag{19}$$

In Eq. (19), $-dp/dx$ is the employed pressure gradient, η is the dynamic viscosity of the liquid, e is the electronic charge, n_i is the number density of the ionic species i, and $\kappa = a_k^2\left(\frac{d}{\sigma a_k^3 N_p \varphi}\right)^2$ is the permeability and $\frac{\sigma a_k^3 N_p \varphi}{d}$ is the volume fraction of the PZI brush layer. For the present study, we consider the cubic profile for φ (see Eq. 14). Of course, the solution of the velocity field u would be sought in the presence of the known distribution of ψ, $n_\pm$, n_{H^+}, and n_{OH^-}.

Using the calculations provided in the previous section, Eq. (19) can be expressed in dimensionless form as follows.

In acidic solution:

$$0 = \frac{d^2\bar{u}}{d\bar{y}^2} - 1 + \frac{\bar{E}_S}{2\bar{\lambda}^2}[\exp(-\bar{\psi}) - (1+\bar{n}_{H^+,\infty})\exp(\bar{\psi}) + \bar{n}_{H^+} - \bar{n}_{OH^-,\infty}\exp\left[\bar{\psi}\left(1+\varphi\frac{\bar{\gamma}_b}{\bar{K}'_b}\right)\right]] - \bar{\alpha}^2\phi^2\bar{u}$$
$$\left[-1 \le \bar{y} \le -1+\bar{d}\right],$$
$$0 = \frac{d^2\bar{u}}{d\bar{y}^2} - 1 + \frac{\bar{E}_S}{2\bar{\lambda}^2}[\exp(-\bar{\psi}) - (1+\bar{n}_{H^+,\infty})\exp(\bar{\psi}) + \bar{n}_{H^+,\infty}\exp(-\bar{\psi}) - \bar{n}_{OH^-,\infty}\exp(\bar{\psi})] \quad \left[-1+\bar{d} \le \bar{y} \le 0\right]. \tag{20}$$

In basic solution:

$$0=\frac{\mathrm{d}^2\bar{u}}{\mathrm{d}\bar{y}^2}-1+\frac{\bar{E}_\mathrm{S}}{2\bar{\lambda}^2}[(1+\bar{n}_{\mathrm{OH}^-,\infty})\exp(-\bar{\psi})-\exp(\bar{\psi})+\bar{n}_{\mathrm{H}^+,\infty}\exp\left[-\bar{\psi}\left(1+\varphi\frac{\bar{\gamma}_\mathrm{a}}{\bar{K}'_\mathrm{a}}\right)\right]-\bar{n}_{\mathrm{OH}^-}]-\bar{\alpha}^2\phi^2\bar{u}$$
$$\left[-1\le\bar{y}\le-1+\bar{d}\right],$$
$$0=\frac{\mathrm{d}^2\bar{u}}{\mathrm{d}\bar{y}^2}-1+\frac{\bar{E}_\mathrm{S}}{2\bar{\lambda}^2}[(1+\bar{n}_{\mathrm{OH}^-,\infty})\exp(-\bar{\psi})-\exp(\bar{\psi})+\bar{n}_{\mathrm{H}^+,\infty}\exp(-\bar{\psi})-\bar{n}_{\mathrm{OH}^-,\infty}\exp(\bar{\psi})]\ \left[-1+\bar{d}\le\bar{y}\le0\right]. \tag{21}$$

In Eqs. (20) and (21), $\bar{u}=\frac{u}{u_{p,0}}$ (where $u_{p,0}=\frac{h^2}{\eta}\frac{\mathrm{d}p}{\mathrm{d}x}$ is pressure-driven velocity scale), $\bar{E}_\mathrm{S}=\frac{E_\mathrm{S}}{E_0}$ (where $E_0=\frac{e\eta u_{p,0}}{\epsilon_0\epsilon_\mathrm{r}k_\mathrm{B}T}=\frac{\mathrm{d}p}{\mathrm{d}x}\frac{eh^2}{\epsilon_0\epsilon_\mathrm{r}k_\mathrm{B}T}$ is the scale of the electric field), and $\bar{\alpha}=\frac{\sigma a_k^2N_p}{\bar{d}}$. $u_\mathrm{r}=\frac{u_{e,0}}{u_{p,0}}$ is taken to be unity, where $u_{e,0}=\frac{k_\mathrm{B}T}{e}\frac{\epsilon_0\epsilon_\mathrm{r}E_0}{\eta}$ is the electroosmotic velocity scale. Solution of Eqs. (20) and (21) is sought in the presence of the following dimensionless boundary conditions:

$$(\bar{u})_{\bar{y}=-1}=0;\left(\frac{\mathrm{d}\bar{u}}{\mathrm{d}\bar{y}}\right)_{\bar{y}=0}=0;\ (\bar{u})_{\bar{y}=(-1+\bar{d})^+}=(\bar{u})_{\bar{y}=(-1+\bar{d})^-};\ \left(\frac{\mathrm{d}\bar{u}}{\mathrm{d}\bar{y}}\right)_{\bar{y}=(-1+\bar{d})^+}=\left(\frac{\mathrm{d}\bar{u}}{\mathrm{d}\bar{y}}\right)_{\bar{y}=(-1+\bar{d})^-}. \tag{22}$$

Of course, the solution of $\bar{u}$ requires the value of the $\bar{E}_\mathrm{S}$. Calculation of $\bar{E}_\mathrm{S}$ is discussed in the following subsection.

2.3 Streaming electric field E_S

To obtain E_S, we consider that the net ionic current (per unit width) i is equal to zero, that is

$$i=2e\int_{-h}^{0}\left(u_+n_+-u_-n_-+u_{\mathrm{H}^+}n_{\mathrm{H}^+}-u_{\mathrm{OH}^-}n_{\mathrm{OH}^-}\right)\mathrm{d}y=0, \tag{23}$$

where u_i $(i=\pm,\mathrm{H}^+,\mathrm{OH}^-)$ is the ion migration velocity, which is expressed as follows:

$$u_i=u+\frac{ez_iE_\mathrm{S}}{f_i}. \tag{24}$$

Here, f_i is the ionic friction coefficient and z_i is the valence for ion i. Substituting Eq. (24) in Eq. (23), we finally obtain the dimensionless streaming electric field as follows.

In acidic solution:

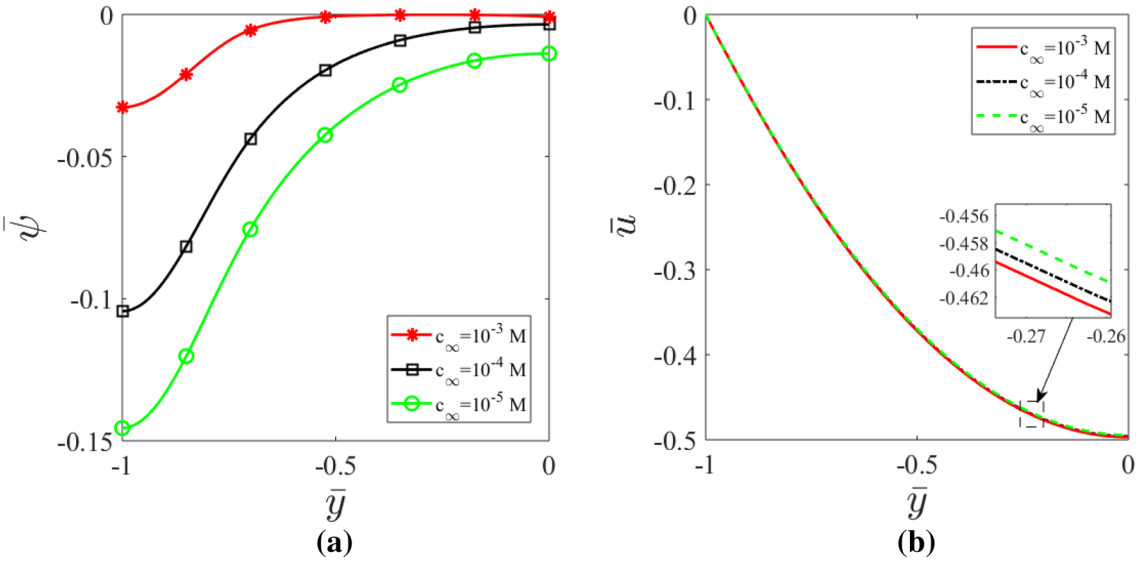

Fig. 3 Transverse variation of **a** $\bar{\psi}$ and **b** $\bar{u}$ for different values of c_∞. Here, we consider $\mathrm{pH}_\infty=10$ (bulk pH). All other parameters are identical to that used in Fig. 2

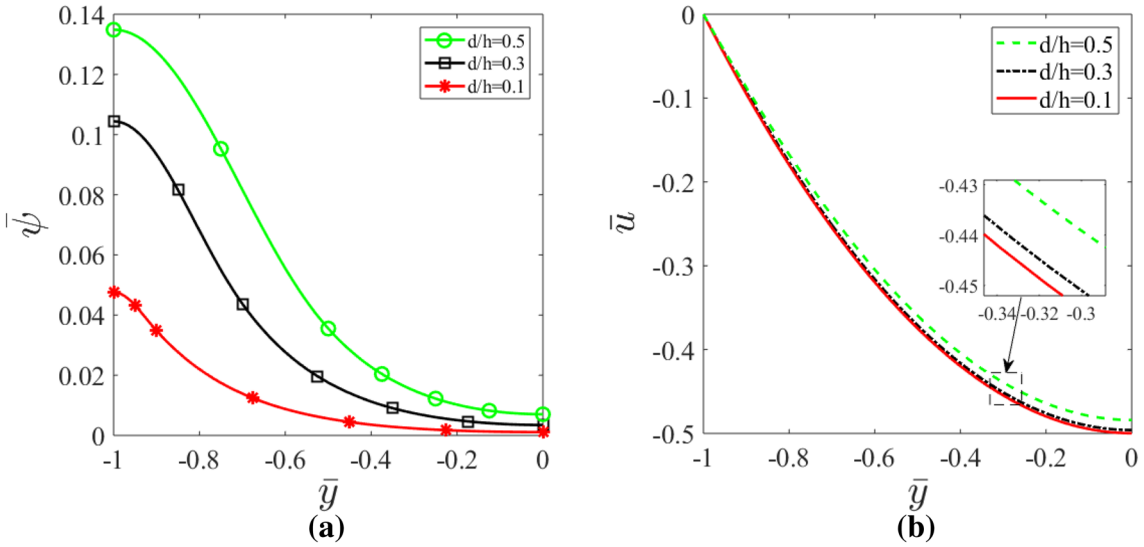

Fig. 4 Transverse variation of **a** $\bar{\psi}$ and **b** $\bar{u}$ for different values of $\bar{d}$. Here, we consider $c_\infty = 10^{-4}$ M. All other parameters are identical to that used in Fig. 2

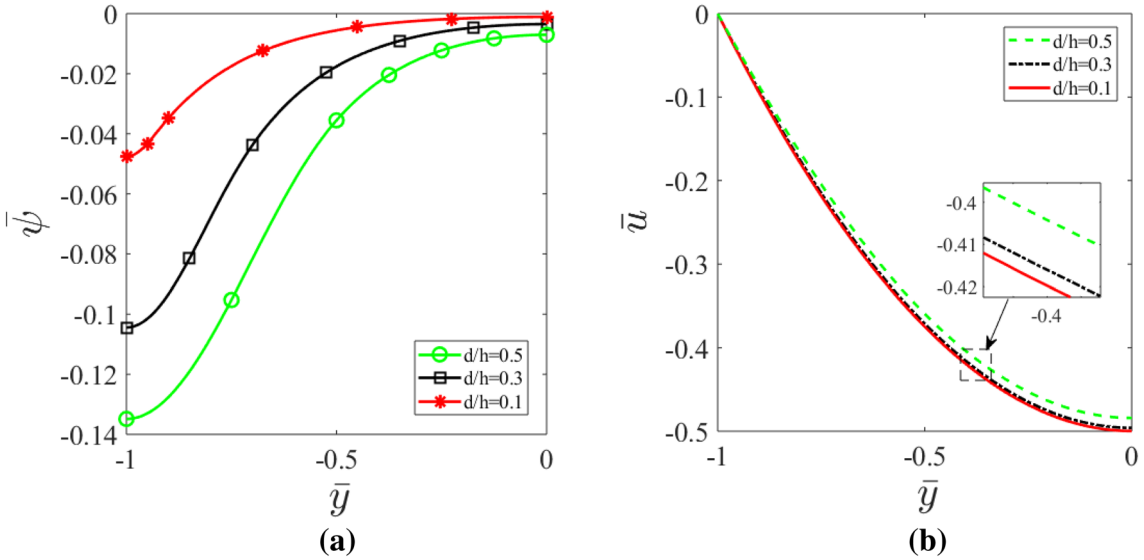

Fig. 5 Transverse variation of **a** $\bar{\psi}$ and **b** $\bar{u}$ for different values of $\bar{d}$. Here, we consider $c_\infty = 10^{-4}$ M. All other parameters are identical to that used in Fig. 3

$$\bar{E}_S = \frac{\int_{-1}^{0} \bar{u}\left[-\exp(-\bar{\psi}) + (1+\bar{n}_{H^+,\infty})\exp(\bar{\psi}) - \bar{n}_{H^+} + \bar{n}_{OH^-}\right]d\bar{y}}{\int_{-1}^{0}[R_+\exp(-\bar{\psi}) + R_-(1+\bar{n}_{H^+,\infty})\exp(\bar{\psi}) + R_{H^+}\bar{n}_{H^+} + R_{OH^-}\bar{n}_{OH^-})]d\bar{y}}. \tag{25}$$

In basic solution:

$$\bar{E}_S = \frac{\int_{-1}^{0} \bar{u}\left[-(1+\bar{n}_{OH^-,\infty})\exp(-\bar{\psi}) + \exp(\bar{\psi}) - \bar{n}_{H^+} + \bar{n}_{OH^-}\right]d\bar{y}}{\int_{-1}^{0}[R_+(1+\bar{n}_{OH^-,\infty})\exp(-\bar{\psi}) + R_-\exp(\bar{\psi}) + R_{H^+}\bar{n}_{H^+} + R_{OH^-}\bar{n}_{OH^-})]d\bar{y}}, \tag{26}$$

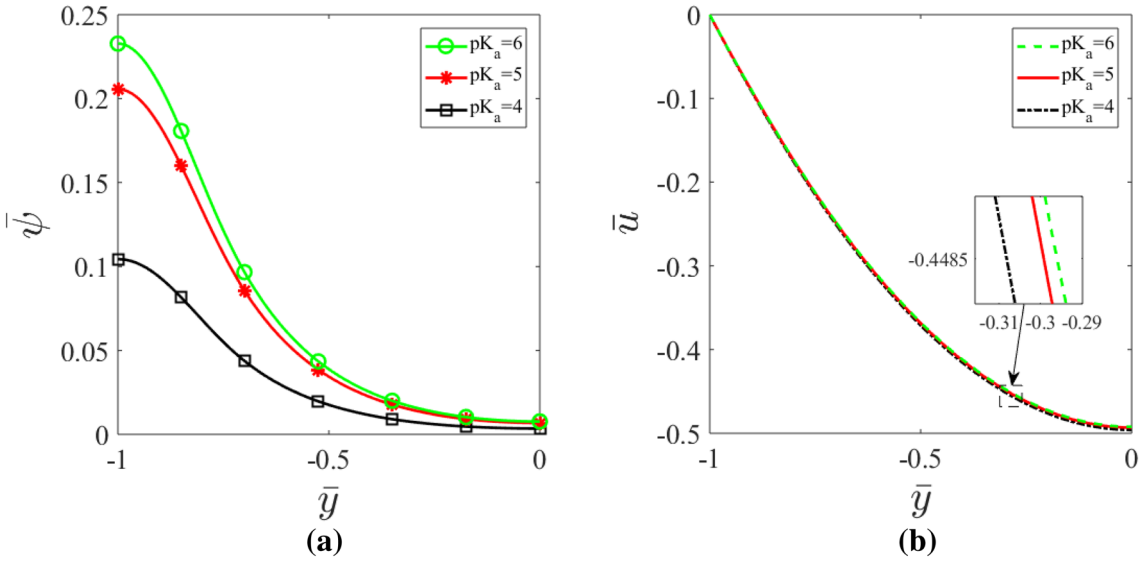

Fig. 6 Transverse variation of **a** $\bar{\psi}$ and **b** $\bar{u}$ for different values of pK_a. Here, we consider $c_\infty = 10^{-4}$ M. All other parameters are identical to that used in Fig. 2

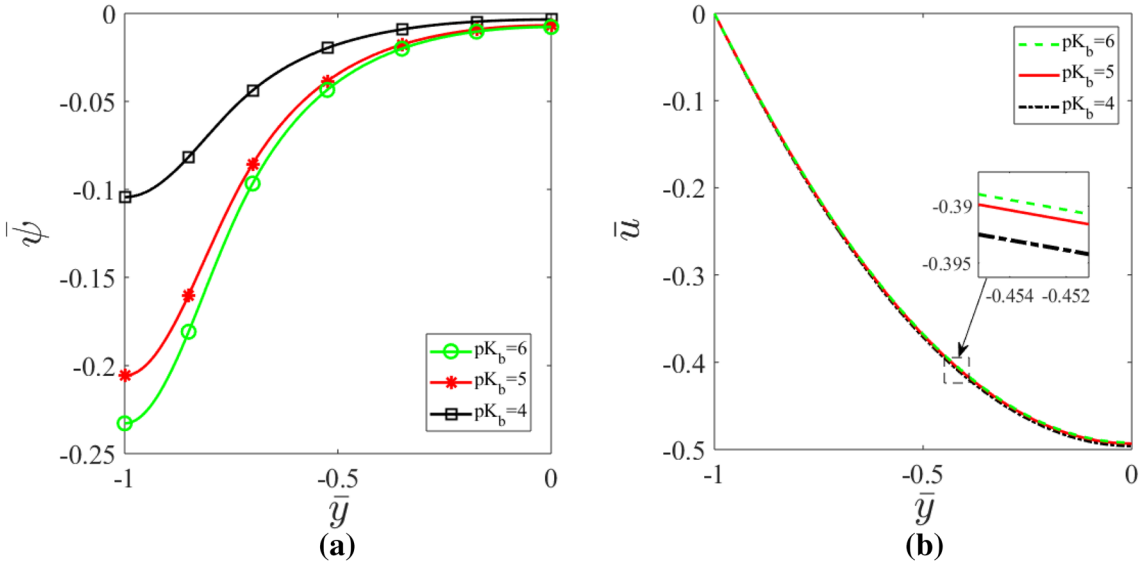

Fig. 7 Transverse variation of **a** $\bar{\psi}$ and **b** $\bar{u}$ for different values of pK_b. Here, we consider $c_\infty = 10^{-4}$ M. All other parameters are identical to that used in Fig. 3

where $R_i = \frac{e^2 z_i^2 \eta}{\epsilon_0 \epsilon_r k_B T f_i}$ is a dimensionless parameter, often interpreted as the inverse of the ionic Peclet number. We take $f = \frac{eE_0}{u_{p,0}} = \frac{e^2 \eta}{\epsilon_0 \epsilon_r k_B T}$. Of course, we would use Eq. (25) in Eq. (20) to obtain the integro-differential equation governing the velocity field $\bar{u}$ within the PZI brush-grafted nanochannel in acidic condition; on the other hand, we would use Eq. (26) in Eq. (21) to obtain the integro-differential equation governing the velocity field $\bar{u}$ within the PZI brush-grafted nanochannel in basic condition. The integro-differential equations for both the cases are solved numerically in the presence of the BCs expressed in Eq. (22). We were the first group to develop and solve such highly involved integro-differential equations for obtaining the streaming electric field and the resulting electrokinetics in nanochannels grafted with charged polyelectrolyte brushes (Chen and Das 2015d; Patwary et al. 2015; Chen et al. 2018)—in this study, we again use that theoretical framework to compute the

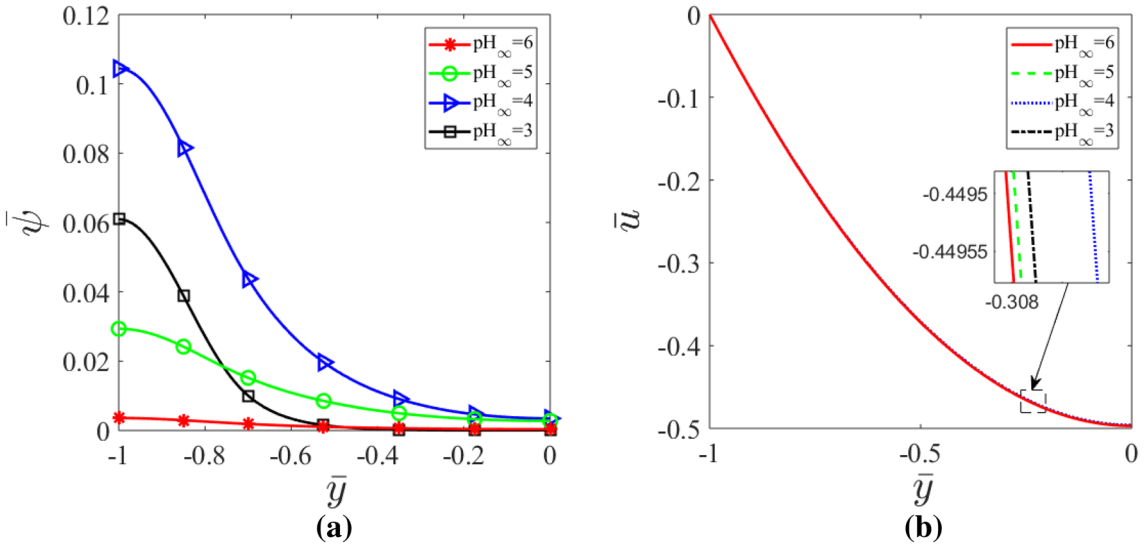

Fig. 8 Transverse variation of **a** $\bar{\psi}$ and **b** $\bar{u}$ for different pH_∞ (bulk pH) values in an acidic solution. Here, we consider $c_\infty = 10^{-4}$ M. All other parameters are identical to that used in Fig. 2

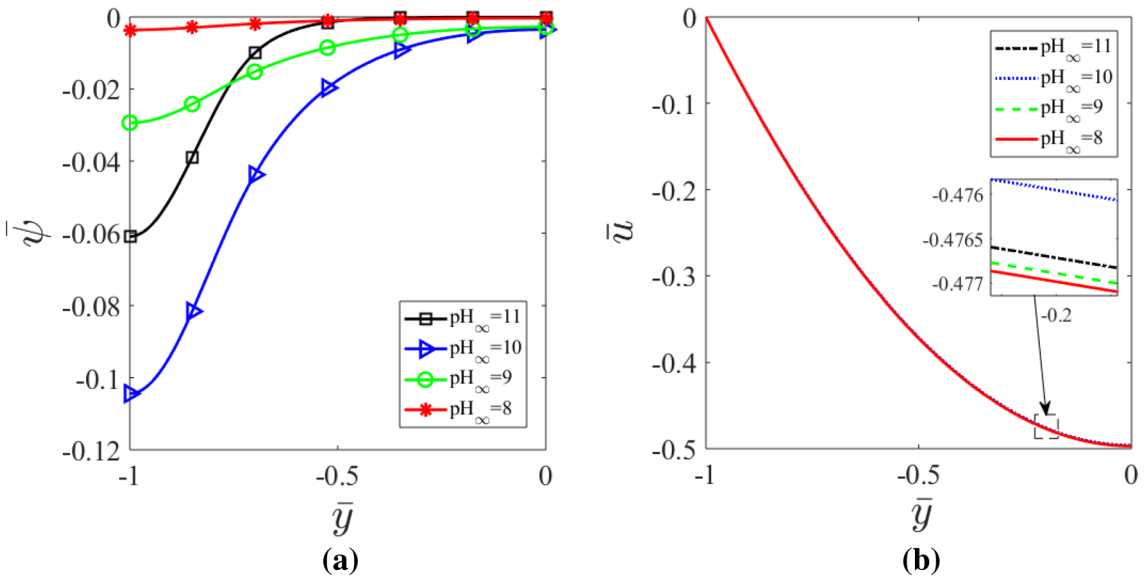

Fig. 9 Transverse variation of **a** $\bar{\psi}$ and **b** $\bar{u}$ for different pH_∞ (bulk pH) values in a basic solution. Here, we consider $c_\infty = 10^{-4}$ M. All other parameters are identical to that used in Fig. 2

induced electrokinetics in nanochannels grafted with the PZI brushes.

2.4 Efficiency of the electrochemomechanical energy conversion

Generation of the nanofluidic streaming current (i_S) and the streaming electric field (E_S) is a process of nanoscale electrochemomechanical energy conversion, since the mechanical energy of the pressure-driven flow and the chemical energy of the EDL are converted to the electrical energy associated with the generation of i_S and E_S. This efficiency ξ of this energy conversion can be expressed as follows:

$$\xi = \frac{P_{out}}{P_{in}}. \tag{27}$$

Here, P_{in} and P_{out} are the input and the output powers (per unit area), expressed as follows:

$$P_{\text{out}} = \frac{1}{4} i_S E_S, \quad P_{\text{in}} = \left| -\frac{\mathrm{d}p}{\mathrm{d}x} \right| Q_{\text{in}}. \tag{28}$$

Here, the streaming current is

$$i_S = 2e \int_{-h}^{0} u\left(n_+ - n_- + n_{H^+} - n_{OH^-}\right) \mathrm{d}y, \tag{29}$$

or in a dimensionless form:

$$\bar{i}_S = \int_{-1}^{0} \bar{u}\left(\bar{n}_+ - \bar{n}_- + \bar{n}_{H^+} - \bar{n}_{OH^-}\right) d\bar{y}, \tag{30}$$

where $\bar{i}_S = \frac{i_S}{2hen_\infty u_{p,0}}$ and Q_{in} is the input volume flow rate per unit width, expressed as follows:

$$Q_{\text{in}} = 2 \int_{-h}^{0} u_p \mathrm{d}y. \tag{31}$$

Here, u_p is the pure pressure-driven velocity field governed by the following equations:

$$\begin{aligned} &\eta \frac{\mathrm{d}^2 u_p}{\mathrm{d}y^2} - \frac{\mathrm{d}p}{\mathrm{d}x} - \frac{\eta}{\kappa} u_p = 0, \qquad \left[-h \le y \le -h + d_0\right], \\ &\eta \frac{\mathrm{d}^2 u_p}{\mathrm{d}y^2} - \frac{\mathrm{d}p}{\mathrm{d}x} = 0, \qquad \left[-h + d_0 \le y \le 0\right]. \end{aligned} \tag{32}$$

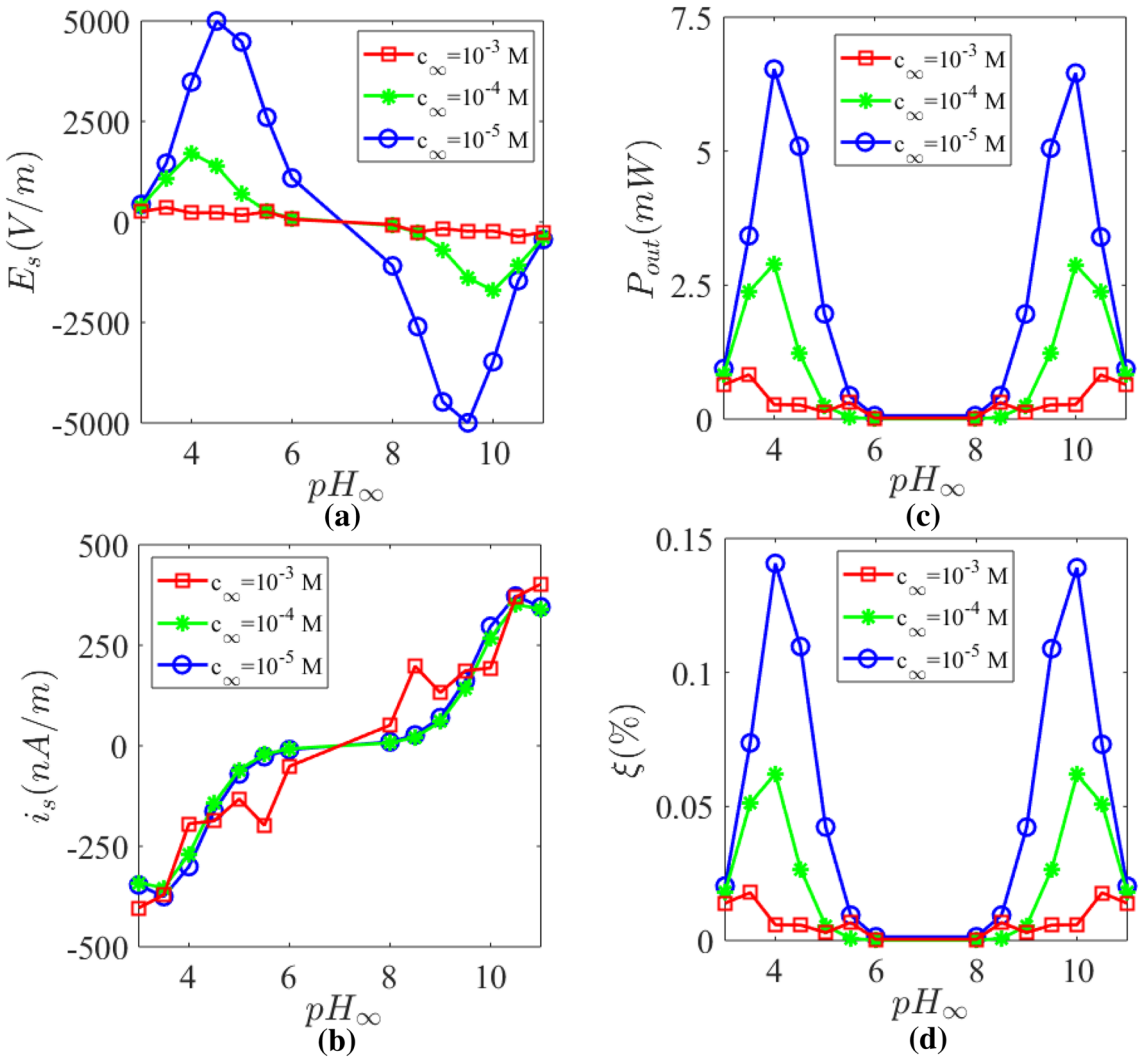

Fig. 10 Variation of **a** streaming electric field E_S, **b** steaming current i_S, **c** output power P_{out}, and **d** electrochemomechanical energy conversion efficiency ξ with pH_∞ for different values of c_∞. To calculate the power, we use $\frac{dp}{dx} = -5 \times 10^8$ Pa/m, $\eta = 8.9 \times 10^{-4}$ Pa s, and consider a nanofluidic chip that is 1 mm×10 cm×10 cm in dimensions (i.e., 1 mm in length and 10 cm in both breadth and width) with a porosity of 0.5. All other parameters are identical to that used in Fig. 2

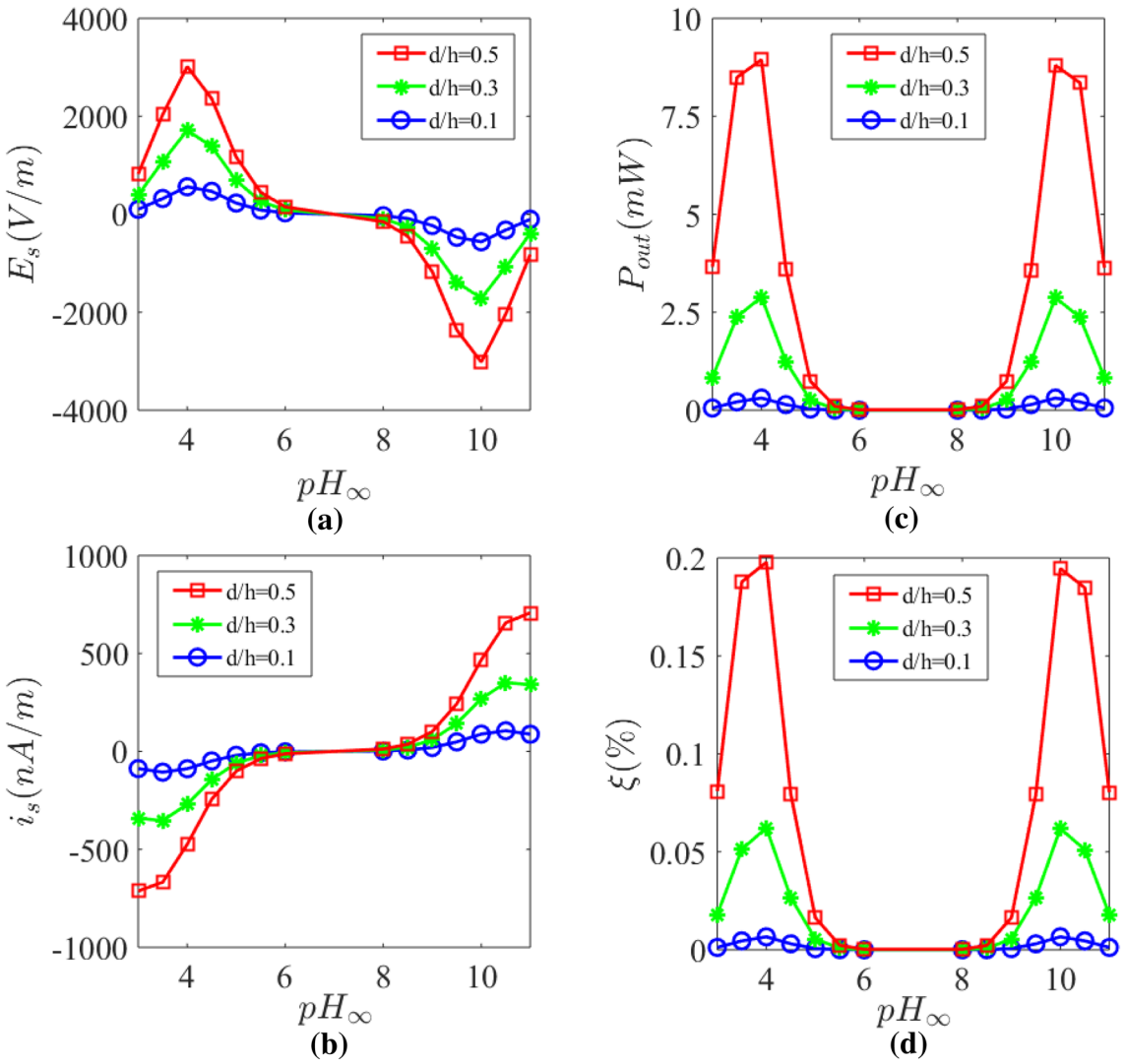

Fig. 11 Variation of **a** E_S, **b** i_S, **c** P_{out}, and **d** ξ with pH_∞ for different values of $\bar{d}$. Here we use $c_\infty = 10^{-4}$ M. All other parameters are identical to that used in Fig. 10

For the acidic solution, we can, therefore, obtain (using Eqs. 25, 27, 28, 30, 31):

$$\xi = \frac{1}{8\bar{\lambda}^2 \int_{-1}^{0} \bar{u}_p \mathrm{d}\bar{y}} \frac{\left[\int_{-1}^{0} \bar{u}\left[-\exp(-\bar{\psi}) + (1+\bar{n}_{\mathrm{H}^+,\infty})\exp(\bar{\psi}) - \bar{n}_{\mathrm{H}^+} + \bar{n}_{\mathrm{OH}^-}\right]\mathrm{d}\bar{y}\right]^2}{\int_{-1}^{0}[\exp(-\bar{\psi}) + (1+\bar{n}_{\mathrm{H}^+,\infty})\exp(\bar{\psi}) + \bar{n}_{\mathrm{H}^+} + \bar{n}_{\mathrm{OH}^-}]\mathrm{d}\bar{y}}. \tag{33}$$

On the other hand, for the basic solution, we can obtain the following (using Eqs. 26, 27, 28, 30, 31). In basic solution:

$$\xi = \frac{1}{8\bar{\lambda}^2 \int_{-1}^{0} \bar{u}_p \mathrm{d}\bar{y}} \frac{\left[\int_{-1}^{0} \bar{u}\left[-(1+\bar{n}_{\mathrm{OH}^-,\infty})\exp(-\bar{\psi}) + \exp(\bar{\psi}) - \bar{n}_{\mathrm{H}^+} + \bar{n}_{\mathrm{OH}^-}\right]\mathrm{d}\bar{y}\right]^2}{\int_{-1}^{0}[\exp(-(1+\bar{n}_{\mathrm{OH}^-,\infty})\bar{\psi}) + \exp(\bar{\psi}) + \bar{n}_{\mathrm{H}^+} + \bar{n}_{\mathrm{OH}^-}]\mathrm{d}\bar{y}}. \tag{34}$$

Of course, both Eqs. (33) and (34) can be simplified to a unique form expressed as follows:

$$\xi = \frac{1}{8\bar{\lambda}^2 \int_{-1}^{0} \bar{u}_p \mathrm{d}\bar{y}} \frac{\bar{i}_S^2}{\bar{i}_C} = \frac{\bar{i}_C \bar{E}_S^2}{8\bar{\lambda}^2 \int_{-1}^{0} \bar{u}_p \mathrm{d}\bar{y}}. \tag{35}$$

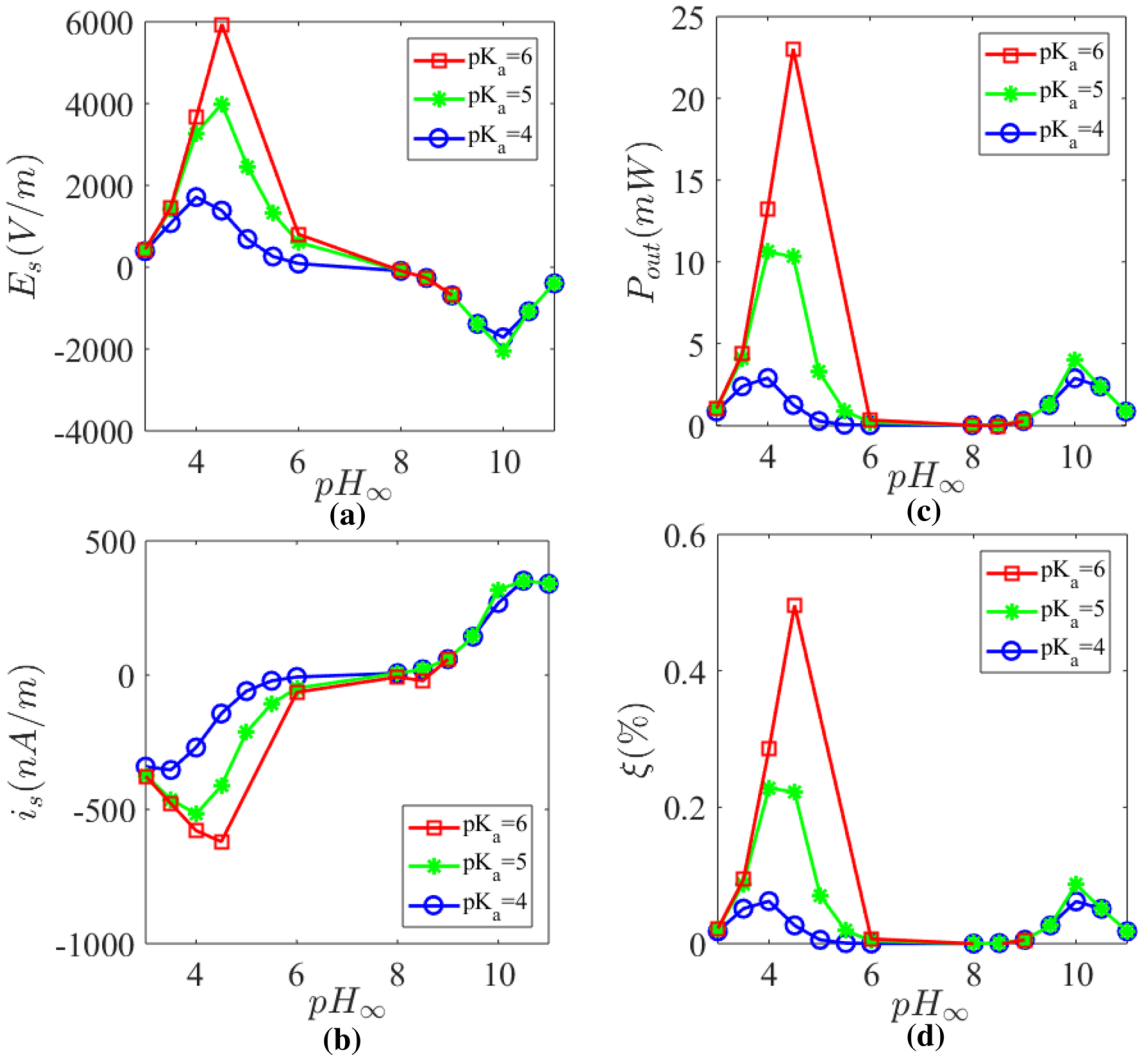

Fig. 12 Variation of **a** E_S, **b** i_S, (**c** P_{out}, and **d** ξ with pH_∞ for different values of pK_a. Here, we use $c_\infty = 10^{-4}$ M. All other parameters are identical to that used in Fig. 10

3 Results

In Figs. 2, 3, 4, 5, 6, 7, 8, and 9, we provide the transverse variation of the dimensionless electrostatic potential ($\bar{\psi}$) and the dimensionless velocity ($\bar{u}$) for different combinations of the system parameters. An acidic solution (characterized by $pH_\infty < 7$) implies the presence of more H^+ ions than OH^- ions. As a consequence, the ionization that produces the BH^+ charged group (this ionization produces more OH^- ions) is more preferred than the ionization that produces the A^- group (this ionization produces more H^+ ions). Therefore, for such a pH (< 7), the PZI attains a net positive charge under identical values of pK_a and pK_b leading to a positive value of the corresponding $\bar{\psi}$. This is evident in Figs. 2a, 4a, 6a, and 8a. On the other hand, a basic solution (characterized by $pH_\infty > 7$) has more OH^- ions than H^+ ions. Accordingly, the ionization that produces H^+ ions (i.e., the ionization that produces the A^- group of the PZI) is much more preferred than the ionization that produces the OH^- ions (i.e., the ionization that produces the BH^+ group of the PZI). As a consequence, for such a pH_∞ (> 7), the PZI attains a net negative charge under identical values of pK_a and pK_b leading to a negative value of the corresponding $\bar{\psi}$ (see Figs. 3a, 5a, 7a, 9a). For both the cases of positive and negative $\bar{\psi}$, a decrease in the salt concentration (c_∞) increases the magnitude of $\bar{\psi}$. Smaller c_∞ leads to a larger EDL thickness (λ), which would imply a larger $\bar{\psi}$ for a given charge density (σ), attributed to the fact that $d\psi/dy \sim \sigma/(\epsilon_0\epsilon_r) \Rightarrow \psi \sim \sigma\lambda/(\epsilon_0\epsilon_r)$. This is evident in Figs. 2a and 3a. Furthermore, an increase in the relative brush height (or larger d/h value) leads to a larger charge content of the system leading to a greater magnitude

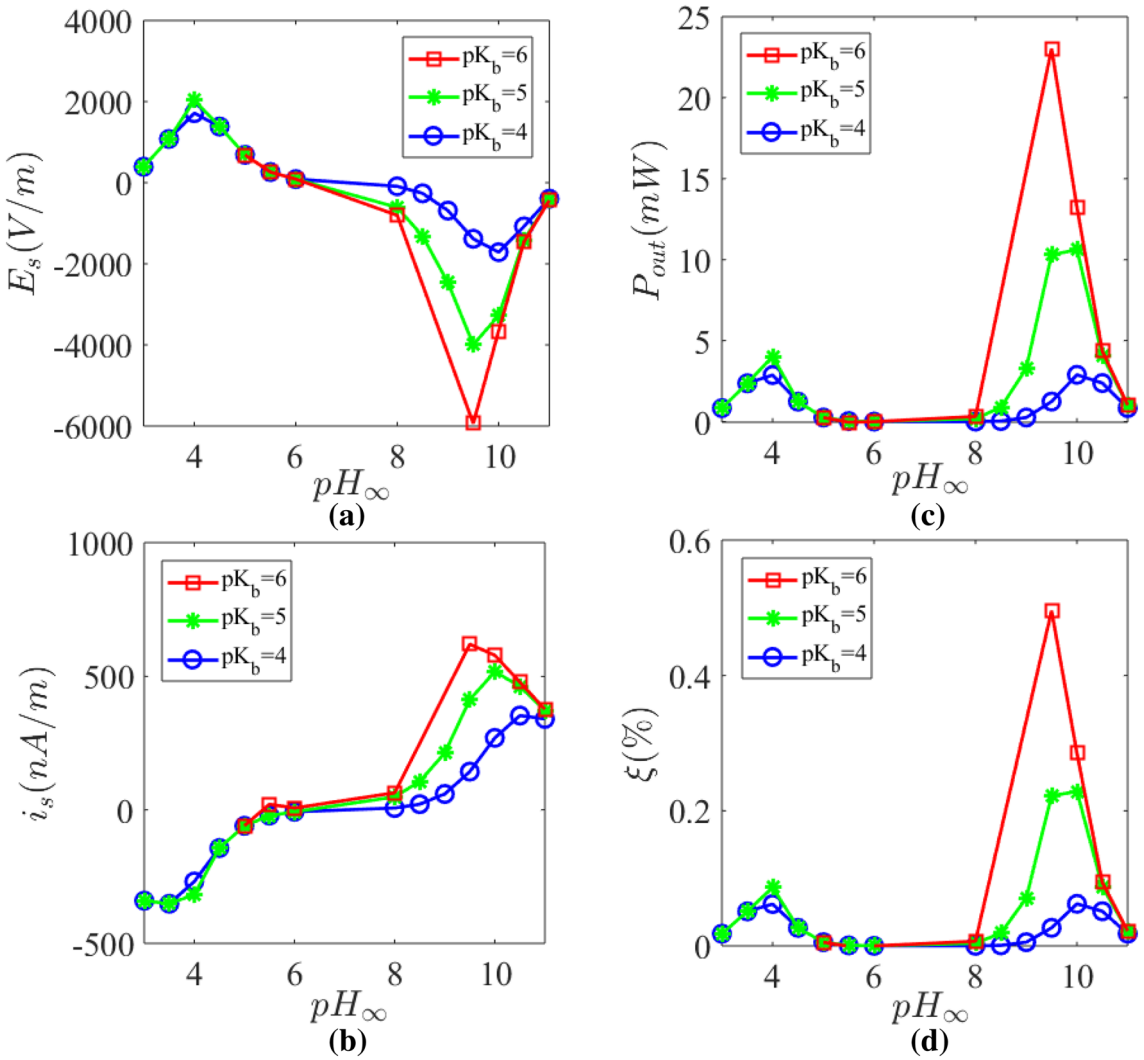

Fig. 13 Variation of **a** E_S, **b** i_S, **c** P_{out}, and **d** ξ with pH_∞ for different values of pK_b. Here, we use $c_\infty = 10^{-4}$ M. All other parameters are identical to that used in Fig. 10

(either positive or negative) of $\bar{\psi}$ (see Figs. 4a, 5a). A larger value of pK_a for the case where the charging of the PZI is dominated by the formation of the positive sites (i.e., the situation that occurs at an acidic pH or $pH_\infty < 7$) implies that the ionization of the PZI to produce the negative sites is retarded and, therefore, leads to a large net positive charge on the PZI and a larger positive magnitude of $\bar{\psi}$. This is depicted in Fig. 6a. Exactly reverse occurs for a basic solution (pH > 7) and larger pK_b. For such a solution, the PZI charge is dominated by the formation of the negative sites and a larger pK_b implies a weaker ionization of the positive sites making the PZI more negative (and hence, $\bar{\psi}$ more negative). This is depicted in Fig. 7a. Finally, in Figs. 8 and 9, we show the effect of the variation in pH_∞. In the acidic range, a progressive lowering of pH_∞ (or a progressive increase in the number of H^+ ions) implies a more retarded ionization of the negative group of the PZI (this ionization produced H^+ ions) implying a larger manifestation of the positive charge of the PZI ensuring a larger positive value of $\bar{\psi}$. This is witnessed for pH_∞ values varying from 6 to 4. However, for pH_∞ 3, we find that the $\bar{\psi}$ becomes smaller than that at pH_∞ 4. The reason is that, since we operate at $c_\infty = 10^{-4}$ M, at pH 3 (or $c_{H^+,\infty} = 10^{-3}$ M), the hydrogen ion concentration dictates the EDL thickness causing a decrease in the EDL thickness as compared to the case when pH_∞ 4. This lowering of the EDL thickness reduces the overall $\bar{\psi}$. This behavior is witnessed in Fig. 8a. On the other hand, in the basic range, a progressive increase in pH_∞ implying a progressive lowering of pOH_∞ (or a progressive increase in the number of OH^- ions) leads to a suppression of the ionization that generates positive charge of the PZI (this ionization also produces the OH^- ion) enforcing a larger negative

charge of the PZI. Therefore, one witnesses a progressively larger negative magnitude of $\bar{\psi}$ as pH_∞ increases from 8 to 10. However, at pH_∞ 11 or pOH_∞ 3, the concentration of the OH^- ions dictates the EDL thickness making the EDL thickness smaller than that for pH_∞ 10 (or pOH_∞ 4) enforcing a reduction in $\bar{\psi}$ (see Fig. 9a).

The part (b) of Figs. 2, 3, 4, 5, 6, 7, 8, and 9 provide the variation of the overall velocity field for the different combination of the system parameters. The overall velocity field is a combination of the pressure-driven transport (caused by the employed pressure gradient) and the induced EOS transport caused by the induced streaming electric field (shown in Figs. 10, 11, 12, 13a). Regardless of the value of pH_∞ (or the corresponding sign of the net charge on the PZI), the EOS transport always opposes the pressure-driven transport and hence reduces the overall transport. Please note that here both the pressure-driven transport and hence the overall transport are positive—however, the net transport appears negative as we non-dimensionalize the velocity field by a characteristic velocity that is negative (i.e., $u_{p,0} = \frac{h^2}{\eta}\frac{dp}{dx} < 0$).

The induced electric field (E_S) driving the EOS transport is positive for the acidic pH and negative for the basic pH (see Figs. 10, 11, 12, 13a). E_S is induced by the downstream migration of the non-zero charge density of the EDL. For the acidic pH, the PZI is positively charged (manifested by a positive magnitude of $\bar{\psi}$); therefore, the counterions will be anions. Thus, the downstream migration of the EDL charge density would imply a net downstream migration of the negative charges, thereby leading to a larger downstream accumulation of the negative charges. Therefore, the net potential will be more positive on the upstream side than the downstream side, ensuring that the electric field is positive (i.e., from left to right). This electric field interacts with the net EDL charge density to induce the EOS transport. The per unit volume EOS body force is $f_{EOS} = e(n_+ - n_-)E_S$. Of course, a positive E_S occurs when $n_- > n_+$ (as already discussed above) ensuring $f_{EOS} < 0$ and hence $u_{EOS} < 0$. For a basic pH, the net PZI charge is negative making the counterions positive, and therefore, the downstream advection of the EDL charge density leads to a downstream accumulation of the positive ions. This ensures that the net potential is more positive downstream, enforcing $E_S < 0$. Of course, as $n_+ > n_-$ for this case, $f_{EOS} = e(n_+ - n_-)E_S < 0$ and $u_{EOS} < 0$ for this case, as well.

A larger magnitude of $\bar{\psi}$ leads to a larger difference between the counterion and coion number density within an EDL, which, in turn, would enforce both a larger magnitude of E_S and an even larger magnitude of f_{EOS}. Therefore, cases with a larger magnitude of $\bar{\psi}$ would result in a larger magnitude of u_{EOS} and, hence, a larger reduction in the overall velocity field. Therefore, we witness a lesser velocity for a weaker salt concentration (see Figs. 2b, 3b), for a larger brush height (see Figs. 4b, 5b), for a larger pK_a for acidic solution (see Fig. 6b), for a larger pK_b for basic solution (see Fig. 7b), for smaller pH_∞ for acidic solution (see Fig. 8b) (except for very small pH_∞, where the hydrogen ion number density dictates the EDL thickness), and for larger pH_∞ for basic solution (see Fig. 9b) (except for very large pH_∞ where the hydroxyl ion number density dictates the EDL thickness).

Figures 10, 11, 12 and 13a provide the variation of the streaming electric field E_S with pH_∞ for different system parameters. We invariably find a positive (negative) E_S for acidic (basic) pH. As we have already discussed above, such a behavior can be attributed to the net positive (negative) charge of the PZI leading to anions (cations) becoming the counterions at an acidic (basic) pH. In addition, all the factors that lead to an enhancement in the magnitude of $\bar{\psi}$ (see Figs. 2, 3, 4, 5, 6, 7, 89a) would augment the magnitude of E_S. Such a connection directly follows from the fact that a larger magnitude of $\bar{\psi}$ would imply a larger difference in the number densities between the counterions and coions, and hence, a larger magnitude of the electrostatic potential difference (caused by the flow-driven downstream accumulation of the counterions) leads to a larger E_S. Therefore, one witnesses a larger magnitude of E_S for a weaker salt concentration (see Fig. 10a), for a larger brush height (see Fig. 11a), for a larger pK_a for an acidic solution (see Fig. 12a), for a larger pK_b for a basic solution (see Fig. 13a), for smaller pH_∞ for acidic solution (see Figs. 10, 11, 12, 13a) (except for very small pH_∞, where the hydrogen ion number density dictates the EDL thickness and this ensures a maximum in the magnitude of E_S at an intermediate pH_∞), and for larger pH_∞ for basic solution (see Figs. 10, 11, 12, 13a) (except for very large pH_∞ where the hydroxyl ion number density dictates the EDL thickness and this ensures a minimum or a negative maximum in the magnitude of E_S at an intermediate pOH_∞). A critical observation from all the E_S plots is a remarkable symmetry (in magnitude) across the pH_∞ spectrum. In other words, we get the same magnitude (with different sign) for the same values of pH_∞ and pOH_∞ (i.e., at large and small pH_∞). This obviously stems from the fact that PZI becomes charged at these extreme pH_∞ values. Therefore, this study points to this unique opportunity where one can attain a large magnitude of E_S for both large and small pH.

Figures 10, 11, 12 and 13b provide the variation of the streaming current i_S with pH_∞ for different system parameters. This streaming current when multiplied by the streaming electric field produces the net output power (see Figs. 10, 11, 12, 13c), which follows the same trend with the different parameters as the electric field E_S. Therefore, we witness an increase in power with weaker c_∞ (see Fig. 10c), for a larger brush height (see Fig. 11c), for a larger pK_a for an acidic pH (see Fig. 12c), for a larger pK_b for a basic solution (see Fig. 13c), for smaller pH_∞ for acidic solution (see

Figs. 10, 11, 12, 13a) (except for very small pH_∞, where the hydrogen ion number density dictates the EDL thickness and this ensures a maximum in the magnitude of power at an intermediate pH_∞), and for larger pH_∞ for basic solution (see Figs. 10, 11, 12, 13a) (except for very large pH_∞ where the hydroxyl ion number density dictates the EDL thickness and this ensures a minimum or a negative maximum in the magnitude of power at an intermediate pOH_∞). Very much like E_S, here too, we ensure a large P for both large and small pH_∞. Finally, in Figs. 10, 11, 12 and 13d, we show the variation in the efficiency ξ in the electrokinetic (or electrochemomechanical) energy conversion. The trend with respect to different parameters is exactly identical to that of the power variation. Most importantly, here too, we ensure a significant conversion efficiency for both large and small pH.

4 Discussions

4.1 Neglecting the PE brush configurational details

In the development of our theoretical model, we have neglected the configurational details of the PE brush. In other words, we have assumed a constant salt-concentration-independent height of the PE brush while developing our model. As we have established in our previous papers (Chen and Das 2015a; Li et al. 2016), such an assumption is only valid if the factors dictating the PE brush configuration [namely the elastic (F_{el}) and the excluded volume (F_{EV}) energies] are decoupled from the corresponding electrostatic effects [namely, the energy associated with the PE charge (F_{elec}) and that associated with the induced EDL (F_{EDL})]. Such decoupling is possible if either $F_{el} + F_{EV} \gg F_{elec} + F_{EDL}$ (which occurs when $\sigma \gg \sigma_c$) or $F_{el} + F_{EV} \ll F_{elec} + F_{EDL}$ (which occurs when $\sigma \ll \sigma_c$). Here, σ is the grafting density and $\sigma_c \approx a^{-1}t^{-1}$ (where a is the Kuhn length and t is the thickness of the polymer brush molecule) is the critical grafting density. Here, we assume that either of these conditions ($\sigma \gg \sigma_c$ or $\sigma \ll \sigma_c$) has been satisfied. Of course, in addition to the above conditions, we need additional constraint on the value of σ. For example, we need to ensure that σ is always large enough to ensure that the grafted polymers may form the brushes, i.e., $\sigma \gg a^{-2}N^{-6/5}$ (Chen and Das 2015a). Furthermore, σ needs to be small enough to ensure that the grafted brushes on opposing nanochannel walls do not interpenetrate, i.e., $\sigma \ll h^3a^{-4}N^{-3}t^{-1}$ (Chen and Das 2015a). Therefore, in summary, our model is valid for $\sigma \ll \sigma_c$ or $\sigma \gg \sigma_c$ and $a^{-2}N^{-6/5} \ll \sigma \ll h^3a^{-4}N^{-3}t^{-1}$ (Chen and Das 2015a).

It is worthwhile to note here that most of the papers studying the liquid flows in nanochannels grafted with PE brushes have considered such salt-concentration-independent brush height (Chanda et al. 2014; Chen and Das 2015d, b; Patwary et al. 2015; Poddar et al. 2016; Milne et al. 2014; Zhou et al. 2016; Yeh et al. 2012b, a; Benson et al. 2013; Zhou et al. 2016; Li et al. 2016; Cao and You 2016; Li et al. 2017) (or the brush height in the decoupled regime). Our paper (Chen and Das 2015a) unraveled, for the first time, the physical conditions under which such decoupling is allowed. In another paper (Li et al. 2016), we provided the examples of experimental studies (Hoffmann et al. 2009; Guo and Ballauff 2000; Wang et al. 2010; Guo and Ballauff 2001) where the above condition of decoupling can be safely employed while describing the PE brush electrostatics. In a recent couple of papers, we have considered a simplistic system (a nanochannel grafted with end-charged brushes) and have provided, for the first time, the calculations for the liquid flows in PE brush-grafted nanochannels where the brush configuration is obtained through a self-consistent thermodynamic analysis (Chen et al. 2018; Chen and Das 2017b). In these papers, we employed the Alexander–de-Gennes model (Alexander 1977; Gennes 1976, 1980) to describe the monomer configuration. Such a situation was afforded by the fact that the PE charge was localized at the non-grafted end of the brush. On the other hand, for the present case where we consider a backbone-charged pH-responsive brush, such simplistic modeling will not be possible and any thermodynamically self-consistent approach would necessitate an analysis that remains missing in the literature despite the significant efforts by the previous researchers (Zhulina and Borisov 2011). In one of our papers (Chen and Das 2015c), we pinpoint that this lacuna stems from considering a Boltzmann distribution description of the hydrogen ions even within the PE brush layer. Therefore, a self-consistent analysis for the present problem would first require a self-consistent thermodynamic analysis of the pH- and pOH-responsive PZI brushes, which is beyond the scope of the present study.

4.2 Choice of the cubic monomer density distribution

Despite considering a decoupled regime, we would still need to know the dimensionless distribution of the PZI chargeable sites φ along the height of the PE brush. In several of our previous papers, we have described the need for considering a *non-unique* cubic distribution of these chargeable sites to ensure a continuity in the hydrogen and hydroxyl ion concentration distribution (Chen and Das 2015b, c; Li et al. 2016; Patwary et al. 2015). This continuity would have been achieved by default had we been able to obtain a fully self-consistent thermodynamic description of the pH-responsive PE brushes. No study has been able to achieve that yet. Under these circumstances, the consideration of this cubic monomeric distribution is the best description of φ that one might achieve for a pH-responsive PE brush.

4.3 Calculation of maximum output power

Figures 10c, 11c, 12c, and 13c provide the variation of the maximum output power using the expression for P_{out} in Eq. (28). To obtain these output power values, we consider a nanofluidic chip consisting of several nanochannels (each of half height 100 nm and grafted with the PZI brushes). The nanofluidic chip is 1 mm in length and 10 cm in both height and width, with a porosity of 0.5. Consequently, the total number of nanochannels present in the chip is 10 cm× 0.5/(2×100 nm) =2.5 $\times 10^5$. The applied pressure gradient is considered to be 5×10^8 Pa/m. This is a reasonable pressure gradient that can be achieved by applying a pressure drop of 5 bar across the chip of length 1 mm. The previous experiments on nanofluidic transport have achieved similar pressure drops across millimetric lengths (Heyden et al. 2005, 2006b). In the caption of Fig. 10, we have reported these numbers. We repeat them here for the sake of clarity. We also note here that we have previously provided such estimates of power generation at the chip scale using nanofluidic energy conversion in nanochannels grafted with end-charged PE brushes with pH-independent charges in the presence of realistic pressure drops (Chen et al. 2018).

5 Conclusions

Here, for the first time, we propose a design that uses a PZI brush-grafted nanochannel for the electrokinetic energy conversion. The unique ability of the PZI to express significant (but opposite charges) at extreme ends of the pH spectrum has been leveraged in this design to generate electrokinetic power from a pressure-driven transport across a wide range of pH spectrum. Typically, the pH responsiveness of nanochannels (with and without the PE brush grafting) enforces a narrow operating pH window for the maximum power generation. Use of PZI brushes expands that window and allows a large power generation across wide ranges (both large and small) pH values.

References

Alexander S (1977) Polymer adsorption on small spheres. A scaling approach. J Phys 38:977

Ali M, Schiedt B, Healy K, Neumann R, Ensinger W (2008) Modifying the surface charge of single track-etched conical nanopores in polyimide. Nanotechnology 19:085713

Ali M, Yameen B, Neumann R, Ensinger W, Knoll W, Azzaroni O (2008) Biosensing and supramolecular bioconjugation in single conical polymer nanochannels. Facile incorporation of biorecognition elements into nanoconfined geometries. J Am Chem Soc 130:16351

Ali M, Ramirez P, Mafe S, Neumann R, Ensinger W (2009) A pH-tunable nanofluidic diode with a broad range of rectifying properties. ACS Nano 3:603

Ali M, Schiedt B, Neumann R, Ensinger W (2010a) Biosensing with functionalized single asymmetric polymer nanochannels. Macromol Biosci 10:28

Ali M, Yameen B, Cervera J, Ramirez P, Neumann R, Ensinger W, Knoll W, Azzaroni O (2010b) Layer-by-layer assembly of polyelectrolytes into ionic current rectifying solid-state nanopores: insights from theory and experiment. J Am Chem Soc 132:8338

Azzaroni O, Brown AA, Huck WTS (2006) UCST wetting transitions of polyzwitterionic brushes driven by self-association. Angew Chem Int Ed 118:1802

Baldessari F, Santiago JG (2008) Electrokinetics in nanochannels: part I. Electric double layer overlap and channel-to-well equilibrium. J Colloid Interface Sci 325:526

Behrens SH, Grier DG (2001) The charge of glass and silica surfaces. J Chem Phys 115:6716

Benson L, Yeh L-H, Chou T-H, Qian S (2013) Field effect regulation of donnan potential and electrokinetic flow in a functionalized soft nanochannel. Soft Matter 9:9767

Cao Q, You H (2016) Electroosmotic flow in mixed polymer brush-grafted nanochannels. Polymers 8:438

Chanda S, Sinha S, Das S (2014) Streaming potential and electroviscous effects in soft nanochannels: towards designing more efficient nanofluidic electrochemomechanical energy converters. Soft Matter 10:7558

Chen G, Das S (2015a) Scaling laws and ionic current inversion in polyelectrolyte-grafted nanochannels. J Phys Chem B 119:12714

Chen G, Das S (2015b) Electroosmotic transport in polyelectrolyte-grafted nanochannels with pH-dependent charge density. J Appl Phys 117:185304

Chen G, Das S (2015c) Electrostatics of soft charged interfaces with pH-dependent charge density: effect of consideration of appropriate hydrogen ion concentration distribution. RSC Adv 5:4493

Chen G, Das S (2015d) Streaming potential and electroviscous effects in soft nanochannels beyond Debye–Hckel linearization. J Colloid Interface Sci 445:357

Chen G, Das S (2017a) Thermodynamics, electrostatics, and ionic current in nanochannels grafted with pH-responsive end-charged polyelectrolyte brushes. Electrophoresis 38:720

Chen G, Das S (2017b) Massively enhanced electroosmotic transport in nanochannels grafted with end-charged polyelectrolyte brushes. J Phys Chem B 121:3130

Chen M, Briscoe WH, Armes SP, Klein J (2009) Lubrication at physiological pressures by polyzwitterionic brushes. Science 323:1698

Chen M, Briscoe WH, Armes SP, Cohen H, Klein J (2011) Polyzwitterionic brushes: extreme lubrication by design. Eur Polym J 47:511

Chen G, Sachar HS, Das S (2018) Efficient electrochemomechanical energy conversion in nanochannels grafted with end-charged polyelectrolyte brushes at medium and high salt concentration. Soft Matter 14:5246

Cheng N, Brown AA, Azzaroni O, Huck WTS (2008) Thickness-dependent properties of polyzwitterionic brushes. Macromolecules 41:6317

Daiguji H, Yang P, Szeri AJ, Majumdar A (2004) Electrochemomechanical energy conversion in nanofluidic channels. Nano Lett 4:2315

Das S, Guha A, Mitra SK (2013) Exploring new scaling regimes for streaming potential and electroviscous effects in a nanocapillary with overlapping electric double layers. Anal Chim Acta 804:159

Das S, Chanda S, Eijkel JCT, Tas NR, Chakraborty S, Mitra SK (2014) Filling of charged cylindrical capillaries. Phys Rev E 90:043011

Das S, Banik M, Chen G, Sinha S, Mukherjee R (2015) Polyelectrolyte brushes: theory, modelling, synthesis and applications. Soft Matter 11:8550

de Gennes P-G (1976) Scaling theory of polymer adsorption. J Phys 37:1443
de Gennes P-G (1980) Conformations of polymers attached to an interface. Macromolecules 13:1069
de Groot GW, Santonicola MG, Sugihara K, Zambelli T, Reimhult E, Vrös J, Vancso GJ (2013) Switching transport through nanopores with pH-responsive polymer brushes for controlled ion permeability. ACS Appl Mater Interface 5:1400
Fidale LC, Nikolajski M, Rudolph T, Dutz S, Schacher FH, Heinze T (2013) Hybrid Fe_3O_4@ amino cellulose nanoparticles in organic mediaheterogeneous ligands for atom transfer radical polymerizations. J Colloid Interface Sci 390:25
Gilles FM, Tagliazucchi M, Azzaroni O, Szleifer I (2016) Ionic conductance of polyelectrolyte-modified nanochannels: nanoconfinement effects on the coupled protonation equilibria of polyprotic brushes. J Phys Chem C 120:4789
Guo X, Ballauff M (2000) Spatial dimensions of colloidal polyelectrolyte brushes as determined by dynamic light scattering. Langmuir 16:8719
Guo X, Ballauff M (2001) Spherical polyelectrolyte brushes: comparison between annealed and quenched brushes. Phys Rev E 64:051406
Higaki Y, Kobayashi M, Murakami D, Takahara A (2016) Anti-fouling behavior of polymer brush immobilized surfaces. Polym J 48:325
Hoffmann M, Jusufi A, Schneider C, Ballauff M (2009) Surface potential of spherical polyelectrolyte brushes in the presence of trivalent counterions. J Colloid Interface Sci 338(566):566
Ilcikova M, Tkac J, Kasak P (2015) Switchable materials containing polyzwitterion moieties. Polymers 7:2344
Knop K, Hoogenboom R, Fischer D, Schubert US (2010) Poly(ethylene glycol) in drug delivery: pros and cons as well as potential alternatives. Angew Chem Int Ed 49:6288
Kobayashi M, Takahara A (2013) Environmentally friendly repeatable adhesion using a sulfobetaine-type polyzwitterion brush. Polym Chem 4:4987
Li F, Jian Y, Chang L, Zhao G, Yang L (2016) Alternating current electroosmotic flow in polyelectrolyte-grafted nanochannel. Colloid Surf B 147:234
Li H, Chen G, Das S (2016) Electric double layer electrostatics of pH-responsive spherical polyelectrolyte brushes in the decoupled regime. Colloid Surf B 147:180
Li F, Jian Y, Xie Z, Liu Y, Liu Q (2017) Transient alternating current electroosmotic flow of a jeffrey fluid through a polyelectrolyte-grafted nanochannel. RSC Adv 7:782
Lin J-Y, Lin C-Y, Hsu J-P, Tseng S (2016) Ionic current rectification in a pH-tunable polyelectrolyte brushes functionalized conical nanopore: effect of salt gradient. Anal Chem 88:1176
Lowe AB, McCormick CL (2006) Polyelectrolytes and polyzwitterions: synthesis, properties, and applications. In: ACS Symposium Series, American Chemical Society
Ma Y, Yeh L-H, Lin C-Y, Mei L, Qian S (2015) pH-regulated ionic conductance in a nanochannel with overlapped electric double layers. Anal Chem 87:4508
Milne Z, Yeh LH, Chou TH, Qian S (2014) Tunable donnan potential and electrokinetic flow in a biomimetic gated nanochannel with ph-regulated polyelectrolyte brushes. J Phys Chem C 118:19806
Milner ST (1991) Polymer brushes. Science 251:905
Monteil C, Bar N, Bee A, Villemin D (2016) An efficient recyclable magnetic material for the selective removal of organic pollutants. Beilstein J Nanotechnol 7:1447
Moya S, Azzaroni O, Farhan T, Osborne VL, Huck WTS (2005) Locking and unlocking of polyelectrolyte brushes: toward the ffabrication of chemically controlled nanoactuators. Angew Chem Int Ed 44:4578
Netz RR, Andelman D (2003) Neutral and charged polymers at interfaces. Phys Rep 380:1
Nguyen T, Xie Y, de Vreede LJ, van den Berg A, Eijkel JCT (2013) Highly enhanced energy conversion from the streaming current by polymer addition. Lab Chip 13:3210
Patwary J, Chen G, Das S (2015) Efficient electrochemomechanical energy conversion in nanochannels grafted with polyelectrolyte layers with pH-dependent charge density. Microfluid Nanofluid 20:37
Poddar A, Maity D, Bandopadhyay A, Chakraborty S (2016) Electrokinetics in polyelectrolyte grafted nanofluidic channels modulated by the ion partitioning effect. Soft Matter 12:5968
Saleh TA, Rachman IB, Ali SA (2017) Tailoring hydrophobic branch in polyzwitterionic resin for simultaneous capturing of Hg(II) and methylene blue with response surface optimization. Sci Rep 7:4573
ShamsiJazeyi H, Miller CA, Wong MS, Tour JM, Verduzco R, ShamsiJazeyi Hadi (2014) Polymer coated nanoparticles for enhanced oil recovery. J Appl Polym Sci 131:40576
Suk JS, Xu Q, Kim N, Hanes J, Ensign LM (2015) PEGylation as a strategy for improving nanoparticle-based drug and gene delivery. Adv Drug Deliv Rev. https://doi.org/10.1016/j:addr.2015.09.012
Tagliazucchi M, Szleifer I (2012) Stimuli-responsive polymers grafted to nanopores and other nano-curved surfaces: structure, chemical equilibrium and transport. Soft Matt. 8:7292
Tagliazucchi M, Azzaroni O, Szleifer I (2010) Responsive polymers end-tethered in solid-state nanochannels: when nanoconfinement really matters. J Am Chem Soc 132:12404
Umehara S, Karhanek M, Davis RW, Pourmand N (2009) Label-free biosensing with functionalized nanopipette probes. Proc Natl Acad Sci 106:4611
Urena-Benavides EE, Lin EL, Foster EL, Xue Z, Ortiz MR, Fei Y, Larsen ES, Kmetz AA, Lyon BA, Moaseri E, Bielawski CW, Pennell KD, Ellison CJ, Johnston KP (2016) Low adsorption of magnetite nanoparticles with uniform polyelectrolyte coatings in concentrated brine on model silica and sandstone. Ind Eng Chem Res 55:1522
van der Heyden FHJ, Stein D, Dekker C (2005) Streaming currents in a single nanofluidic channel. Phys Rev Lett 95:116104
van der Heyden FHJ, Bonthuis DJ, Stein D, Meyer C, Dekker C (2006a) Electrokinetic energy conversion efficiency in nanofluidic channels. Nano Lett 7:2232
van der Heyden FHJ, Stein D, Besteman K, Lemay SG, Dekker C (2006b) Charge inversion at high ionic strength studied by streaming currents. Phys Rev Lett 96:224502
van der Heyden FHJ, Bonthuis DJ, Stein D, Meyer C, Dekker C (2007) Power generation by pressure-driven transport of ions in nanofluidic channels. Nano Lett 7:1022
Vilozny B, Wollenberg AL, Actis P, Hwang D, Singaram B, Pourmand N (2013) Carbohydrate-actuated nanofluidic diode: switchable current rectification in a nanopipette. Nanoscale 5:9214
Wang X, Xu J, Li L, Wu S, Chen Q, Lu Y, Ballauff M, Guo X (2010) Synthesis of spherical polyelectrolyte brushes by thermocontrolled emulsion polymerization. Macromol Rapid Commun 31:1272
Xiao W, Lin J, Li M, Ma Y, Chen Y, Zhang C, Li D, Gu H (2012) Prolonged in vivo circulation time by zwitterionic modification of magnetite nanoparticles for blood pool contrast agents. Contrast Media Mol Imaging 7:320
Xue S, Yeh LH, Ma Y, Qian S (2014) Tunable streaming current in a pH-regulated nanochannel by a field effect transistor. J Phys Chem C 118:6090
Yameen B, Ali M, Neumann R, Ensinger W, Knoll W, Azzaroni O (2009) Single conical nanopores displaying ph-tunable rectifying characteristics. Manipulating ionic transport with zwitterionic polymer brushes. J Am Chem Soc 131:2070
Yameen B, Ali M, Neumann R, Ensinger W, Knoll W, Azzaroni O (2009) Synthetic proton-gated ion channels via single solid-state

nanochannels modified with responsive polymer brushes. Nano Lett 9:2788
Yeh L-H, Zhang M, Hu N, Joo SW, Qian S, Hsu J-P (2012a) Controlling pH-regulated bionanoparticles translocation through nanopores with polyelectrolyte brushes. Anal Chem 84:9615
Yeh L-H, Zhang M, Hu N, Joo SW, Qian S, Hsu J-P (2012b) Electrokinetic ion and fluid transport in nanopores functionalized by polyelectrolyte brushes. Nanoscale 4:5169
Zeng Z, Yeh L-H, Zhang M, Qian S (2015) Ion transport and selectivity in biomimetic nanopores with pH-tunable zwitterionic polyelectrolyte brushes. Nanoscale 7:17020
Zhao Y, Chen Y, Xiong X, Sun X, Zhang Q, Gan Y, Zhang L, Zhang W (2017) Synthesis of magnetic zwitterionichydrophilic material for the selective enrichment of N-linked glycopeptides. J Chromatogr A 1482:23
Zhou C, Mei L, Su Y-S, Yeh L-H, Zhang X, Qian S (2016) Gated ion transport in a soft nanochannel with biomimetic polyelectrolyte brush layers. Sens Actuators B 229:305
Zhulina EB, Borisov OV (2011) Poisson–Boltzmann theory of pH-sensitive (annealing) polyelectrolyte brush. Langmuir 27:10615